

# Catalysis Science & Technology

Accepted Manuscript



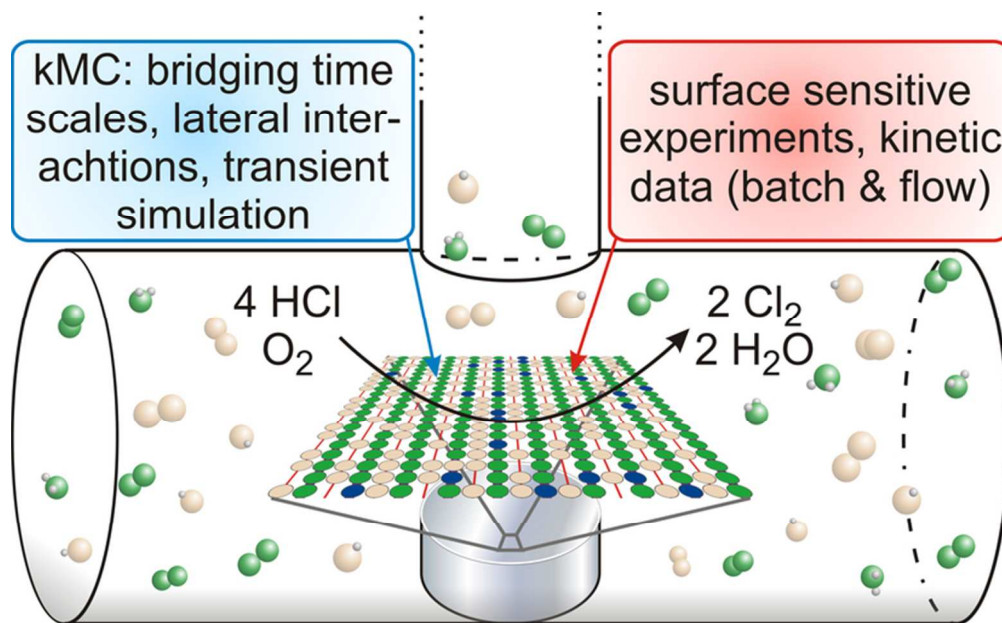
This is an *Accepted Manuscript*, which has been through the RSC Publishing peer review process and has been accepted for publication.

*Accepted Manuscripts* are published online shortly after acceptance, which is prior to technical editing, formatting and proof reading. This free service from RSC Publishing allows authors to make their results available to the community, in citable form, before publication of the edited article. This *Accepted Manuscript* will be replaced by the edited and formatted *Advance Article* as soon as this is available.

To cite this manuscript please use its permanent Digital Object Identifier (DOI®), which is identical for all formats of publication.

More information about *Accepted Manuscripts* can be found in the [Information for Authors](#).

Please note that technical editing may introduce minor changes to the text and/or graphics contained in the manuscript submitted by the author(s) which may alter content, and that the standard [Terms & Conditions](#) and the [ethical guidelines](#) that apply to the journal are still applicable. In no event shall the RSC be held responsible for any errors or omissions in these *Accepted Manuscript* manuscripts or any consequences arising from the use of any information contained in them.



70x42mm (300 x 300 DPI)

# Kinetic Monte Carlo Simulations for Model Catalysis of Heterogeneously Catalyzed Oxidation Reactions

Franziska Hess, and Herbert Over\*

*Dept. of Physical Chemistry, Justus-Liebig-University, Heinrich-Buff-Ring 58,  
D-35392 Gießen, Germany*

\* corresponding author: Herbert.Over@phys.chemie.uni-giessen.de, Fax: ++49-641-9934559

## Abstract:

In this perspective, we focus on the catalyzed oxidation of CO and HCl over the model catalyst RuO<sub>2</sub>(110) and how the kinetics of these reactions can be modeled by kinetic Monte Carlo (kMC) simulations. Assuming the reaction mechanism is known, the critical parameters entering the kMC simulations include the activation and adsorption energies as well as interaction energies between the adsorbed species and the diffusion barriers. This input parameter set can either be determined by using dedicated coadsorption experiments or by calculations from electronic structure theory. Critical comparison of kMC results with on-line kinetic and in-situ spectroscopic experiments enables the assessment of a proposed reaction mechanism. Transient rather than steady state experiments are of particular importance for this purpose. Only the inclusion of lateral interactions among the reaction intermediates allows for the determination of an apparent activation energy which is consistent with the experiment. For the case of CO oxidation over RuO<sub>2</sub>(110) we compare the results of kMC with those based on the mean field approach, the standard method of microkinetic modeling. It turns out that for realistic reaction conditions for the CO oxidation over RuO<sub>2</sub>(110) both methods can equally well describe experimental kinetic data if lateral repulsion is included in the model. However, if one-dimensional confinement is encountered such as with the HCl oxidation reaction over RuO<sub>2</sub>(110), then kMC is the preferred method for microkinetic modeling.

## 1. Introduction

One of the great challenges in chemistry is the formulation of the mechanism of a complex reaction consisting of a sequence of elementary steps.<sup>1, 2</sup> But even if we know all elementary reaction steps, we still do not know how these reaction steps will lead to the observed kinetics of the overall reaction under various reaction conditions. Here, microkinetic (MK) modeling is called for in which the intricate interplay of all reaction steps are explicitly taken into account, based on known activation energies and the frequency factors.<sup>3, 4</sup>

For the case of a heterogeneously catalyzed gas phase reaction the set of elementary reaction steps includes processes of adsorption, desorption, dissociation, recombination and diffusion of molecules and fragments on the catalyst's surface.<sup>5</sup> With surface science methods applied to model catalysts of well-defined atomic structure, in particular single crystalline surfaces, we have access to these elementary steps. With spectroscopic and atomically-resolved imaging methods we can identify reaction intermediates on the model catalyst surface and with well-designed temperature programmed reaction experiments together with state-of-the-art electronic structure calculations the involved activation barriers can be determined.<sup>6</sup> Microkinetic modeling provides simulated kinetic data for various reaction conditions ranging from  $10^{-9}$  mbar to practical pressure of the order of 1...100 bar which can ultimately be compared with kinetic data from experiments, thereby bridging the so-called pressure gap and being able to describe the chemical kinetics of practical catalysts.<sup>7</sup> We may note that a direct inversion of experimental kinetic data to retrieve the activation barriers of the elementary steps by MK modeling constitutes an ill-defined problem for complex reactions as different activation barriers may lead to identical overall kinetics, manifesting a fundamental problem of kinetics.<sup>1</sup>

There are various ways to perform MK modeling. The simplest one is based on a mean field approach (MF)<sup>3</sup> in which only the coverages and not the actual surface configurations of reaction intermediates on the catalyst surface enter the simulations. Recall that MF assumes an ideal mixture of the adsorbed reactants on the catalyst surface, an assumption which is frequently not met on the catalyst surface as pointed out by Ertl and Engel.<sup>8, 9</sup>

A higher level of sophistication is reached in MK when the surface configurations are explicitly taken into account such as in kinetic Monte Carlo simulations (kMC). Kinetic MC is superior over MF whenever heterogeneities are present on the surface, such as phase separation, ordering of the reaction intermediates, 1-dimensionality or high diffusion barriers. For low surface coverages of the reaction intermediates, however, both MF and kMC come to comparable conclusions.

In this perspective, we shall discuss microkinetic modeling via kMC and how to use this powerful tool in model catalysis research, concentrating on reaction systems which we have studied thoroughly over the past couple of years. The surface we focus on is RuO<sub>2</sub>(110) which is considered to be the model catalyst for late transition metal oxides.<sup>10</sup> The particular reactions considered here include the catalyzed oxidation of CO and HCl.

## 2. Kinetic Monte-Carlo method

An accurate and reasonably fast way to follow the time evolution of a system of chemically reacting molecules on the catalyst's surface is provided by kinetic Monte Carlo simulations (kMC)<sup>11-16</sup> which account for fluctuations, correlations and the spatial distribution of the reaction intermediates on the surface. In kMC simulations, the RuO<sub>2</sub>(110) surface is represented by a periodic lattice consisting of a two dimensional array of on-top sites (1f-cus-Ru) and bridge sites (connecting two 2f-cus Ru sites) (cf. Fig. 1) which can either be vacant or accommodate the reactants/intermediates during the simulation, depending on the applied reaction conditions.

Kinetic MC simulations presented in this perspective take explicitly into account the interaction between the molecules, the diffusion of the intermediates on the surface, adsorption/ desorption of the reactants/intermediates including different site demands and the activation barriers for elementary reaction steps. Within the transition state theory, the kinetics of elementary steps are determined by the activation energy and the frequency factor.<sup>17</sup> The activation barriers of elementary steps in the reverse direction result directly from the detailed balance constraint,<sup>18</sup> ensuring the overall thermodynamic consistency in kMC simulations. The binding energies and the energy barriers can either be determined from dedicated surface science experiments or from density functional theory (DFT) studies. The adsorption processes are treated within the kinetic gas theory, assuming a sticking coefficient of unity.<sup>17</sup> The desorption process of reactants or the product in temperature programmed desorption and reaction (TPD, TPR) is simulated within our kMC approach by using the time-dependent First Reaction Method described by Gillespie<sup>19</sup>, and Jansen<sup>20</sup>. Further details about our kMC approach can be found in Ref. 21.

In general, kinetic MC simulations provide atomic scale information concerning: i) the number of turnovers per active site and second; ii) the spatial distribution of reactants on the surface at a particular time; and iii) the number of elementary recombination steps contributing to the overall reaction rate. In principle also the rate determining step (rds) and the most abundant reaction intermediate (MARI) can be inferred from kMC simulations.

### 3. RuO<sub>2</sub>(110), a model catalyst for oxidation catalysis: Examples

In this chapter we discuss several examples, where kinetic Monte Carlo simulations have been applied to deepen our insight into the catalytic reaction system. The chosen examples are motivated by our own research activity which is related to oxidation catalysis over the model catalyst RuO<sub>2</sub>(110). Besides ample experimental details,<sup>22</sup> there are several kMC studies available in the literature which allow for critical comparison. We shall concentrate on two oxidation reactions, namely the CO oxidation reaction and the HCl oxidation reaction. While the CO oxidation reaction is prototypical for surface chemistry and model catalysis,<sup>5, 6</sup> the HCl oxidation reaction has become a particularly interesting system over the past years<sup>23, 24</sup> where the interplay of two different active sites and the 1-dimensionality at the catalyst surface determine the activity in the oxidative dehydrogenation step on the surface. Before starting with a detailed discussion of the particular reaction systems, we shall briefly summarize atomic details of the catalyst surface RuO<sub>2</sub>(110) which are relevant for the following discussion.

#### 3.1 Model Catalyst: RuO<sub>2</sub>(110)

The stoichiometric rutile (110) surface of RuO<sub>2</sub> exposes two kinds of coordinatively unsaturated surface atoms (O<sub>br</sub> and 1f-cus Ru in Fig. 1a) which govern the interaction of the surface with the surrounding reaction gas mixture.<sup>25</sup> The one-fold undercoordinated ruthenium sites (1f-cus Ru) form one-dimensional chains along the [001] direction which are separated by rows of bridging oxygen (O<sub>br</sub>). Occasionally, these O<sub>br</sub> atoms can be partly consumed during the catalytic reaction so that two-fold undercoordinated Ru atoms (2f-cus Ru) become exposed (cf. Fig. 1b). Alternatively, the bridging oxygen atoms can be replaced by CO (cf. Fig. 1c) or Cl atoms.

The 1f-cus Ru sites are the gateway for most of the incident molecules from the gas phase to become accommodated on the surface. For instance, exposing the stoichiometric RuO<sub>2</sub>(110) surface (cf. Fig. 1a) to molecular oxygen will lead to a surface where part of the 1f-cus Ru sites are occupied by on-top sitting oxygen atoms (O<sub>ot</sub>). The O<sub>ot</sub> species represent again undercoordinated surface oxygen atoms (this time two-fold undercoordinated). In another example, the stoichiometric RuO<sub>2</sub>(110) surface is exposed to CO at low temperatures so that the reaction with undercoordinated surface O atoms (O<sub>br</sub> and O<sub>ot</sub>) is suppressed and on-top CO is formed.

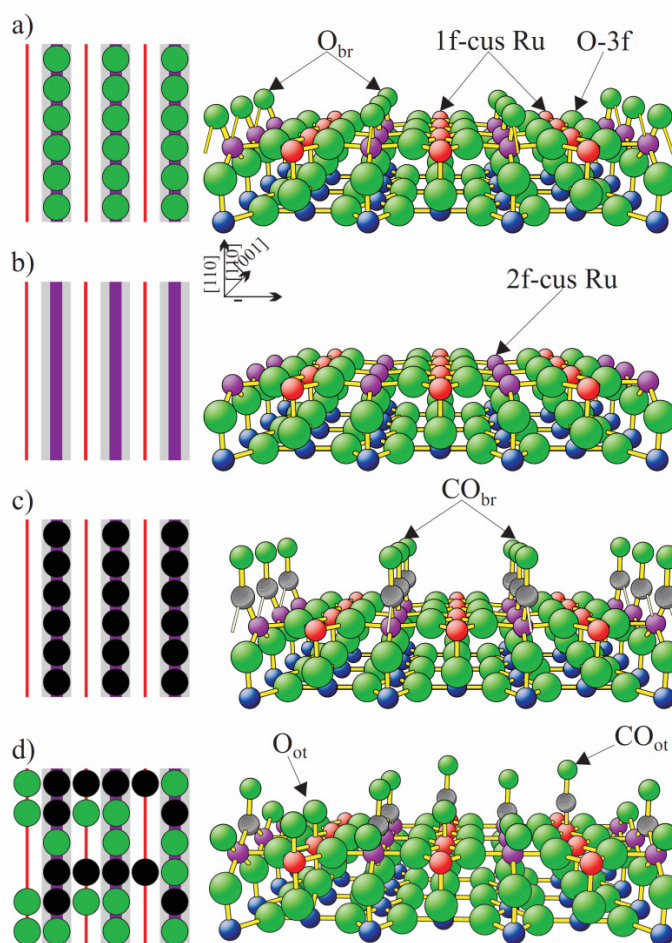


**Fig. 1:** Ball and stick models of the  $\text{RuO}_2(110)$  surface. Green balls stand for O atoms, blue balls for Ru atoms in bulk, red and purple balls for Ru atoms on the surface. At the stoichiometric surface (a) there are two types of chemically active sites, the bridging O atoms ( $\text{O}_{\text{br}}$ ) and the one-fold coordinatively unsaturated Ru sites (1f-cus Ru, red balls). Removal of the  $\text{O}_{\text{br}}$  atoms leads to a mildly reduced  $\text{RuO}_2(110)$  surface (b) where the twofold unsaturated 2f-cus Ru sites are exposed (purple balls). For the rest of the paper, we use a simple representation of the mildly reduced surface by red and purple stripes for the rows of 1f-cus and 2f-cus sites, respectively. Adsorbed O is represented as green balls (a) and adsorbed CO as black balls (c). (d) Example of a coadsorbate structure of bridging O and CO together with on-top CO.

Upon reaction of on-top CO with  $\text{O}_{\text{br}}$ , a vacant bridge site is formed into which CO can readily adsorb, forming a bridging  $\text{CO}_{\text{br}}$ . (cf. Fig. 1c).<sup>26-28</sup> Since deeper reduction of  $\text{RuO}_2(110)$  beyond the replacement or consumption of bridging O by reactant molecules is not considered, the periodic lattice for the kMC simulations is chosen to consist of alternating rows of 1f-cus Ru and 2f-cus Ru (cf. Fig. 1b), which can both be occupied by reactants from the gas phase, preferentially in on-top position over 1f-cus Ru (red balls) and bridging position above neighboring 2f-cus Ru sites (purple balls).

To facilitate easy visualization of surface configurations as provided by the kMC simulations, these rows of 1f-cus Ru and 2f-cus Ru are represented by thin red and thick

purple lines, respectively (cf. Fig. 1, left side), while adsorbates are indicated as small balls (oxygen: green, CO: black, Cl: grey). For illustration, the mixed surface structure consisting of O and CO in bridge sites and on-top  $\text{CO}_{\text{ot}}$  along the cus-Rus rows are depicted in this abbreviated version in comparison with a full stick and ball presentation (cf. Fig. 1d).

## 3.2 CO Oxidation at $\text{RuO}_2(110)$

### 3.2.1 Molecular insight into the elementary processes during CO Oxidation over $\text{RuO}_2(110)$

On the stoichiometric  $\text{RuO}_2(110)$  surface, CO molecules adsorb strongly (adsorption energy exceeds  $120 \text{ kJ/mol}$ <sup>29</sup>) on-top of the 1f-cus-Ru atoms, while oxygen molecules from the gas phase adsorb dissociatively, requiring two neighboring vacant 1f-cus Ru sites.<sup>30</sup> Therefore, CO and  $\text{O}_2$  compete for the same active sites (1f-cus Ru) on the stoichiometric  $\text{RuO}_2(110)$  surface although with different site demands.

Under typical reaction conditions the  $\text{RuO}_2(110)$  surface offers the adsorbed CO molecule two potentially catalytically active oxygen species to recombine with and to form  $\text{CO}_2$ .<sup>31</sup> Besides the bridging O atoms, the  $\text{RuO}_2(110)$  surface stabilizes an on-top oxygen species, which is by  $150 \text{ kJ/mol}$  more weakly bound to  $\text{RuO}_2$  than the bridging O atoms.<sup>30-33</sup> Besides two undercoordinated surface O-species on the  $\text{RuO}_2(110)$  surface, there are two distinct CO adsorption sites on  $\text{RuO}_2(110)$ , namely the bridging CO ( $\text{CO}_{\text{br}}$ ) and the on-top CO ( $\text{CO}_{\text{ot}}$ ) species. This sums up to four elementary reaction steps for the recombination of CO and O at the  $\text{RuO}_2(110)$  surface:  $\text{CO}_{\text{ot}} + \text{O}_{\text{ot}}$ ,  $\text{CO}_{\text{br}} + \text{O}_{\text{ot}}$ ,  $\text{CO}_{\text{br}} + \text{O}_{\text{br}}$ , and  $\text{CO}_{\text{ot}} + \text{O}_{\text{br}}$ . For all these elementary reaction steps, ample experimental<sup>31, 34</sup> and theoretical data (activation and adsorption energies)<sup>32, 35, 36</sup> are available in the literature.

The elementary steps considered in the kMC simulation of the catalytic CO oxidation on  $\text{RuO}_2(110)$  encompass adsorption, desorption of the reactants CO and  $\text{O}_2$ , diffusion of O and CO on the surface along the [001] and the  $[\bar{1}10]$  directions, and the above-mentioned four elementary steps of CO and O recombination<sup>37</sup>, leading altogether to a set of 21 elementary reaction steps, whose parameter values are summarized in **Table 1**.

### 3.2.2 Experiment-Based Kinetic Monte Carlo Simulations

Recently, an experiment-based kMC approach has been developed and applied to the CO oxidation on  $\text{RuO}_2(110)$ <sup>21</sup>. The guiding principle in obtaining a consistent set of input parameters for the experiment-based kMC simulations was to use dedicated temperature programmed reaction and desorption experiments (TPR, TPD) for each of the elementary

reaction steps of the proposed reaction mechanism by starting from a well-defined and appropriate CO and O containing coadsorbate configuration<sup>31,34</sup>. The binding energies of the adsorbates (O, CO)<sup>29,38</sup> and the reaction barriers of specific elementary reaction steps are determined by analyzing the related TPR/TDS experiments by kMC simulations. Since the number of parameters in these auxiliary kMC simulations of each TPR/TDS experiment is limited to typically two parameters, we do not face any problem with the inversion problem of microkinetic modeling. The diffusion barriers have been adopted from DFT calculations. All these parameters are compiled in **Table 1** (second column) and serve as the input parameter set for the kMC simulations of the CO oxidation reaction on RuO<sub>2</sub>(110) without any further adjustable parameter.

**Table 1:** List of elementary steps at the surface considered in the kMC simulations of the CO oxidation reaction over RuO<sub>2</sub>(110). The experiment-based kMC is based on the energies given in the second column while DFT-based kMC are based on Kiejna and Seitsonen's parameter sets. Activation energies are given in kJ/mol.

Elementary step	Activation barrier (energy in kJ/mol)		
	Expt. Based kMC <sup>21</sup>	Kiejna data set <sup>35</sup>	Seitsonen data set <sup>36</sup>
P <sub>1</sub> : Adsorption: O <sub>ot</sub>	0 <sup>38</sup>	0	0
P <sub>2</sub> : Adsorption: O <sub>br</sub>	0 <sup>30</sup>	0	0
P <sub>3</sub> : Adsorption: CO <sub>ot</sub>	0 <sup>29</sup>	0	0
P <sub>4</sub> : Adsorption: CO <sub>br</sub>	0 <sup>39</sup>	0	0
P <sub>5</sub> : Desorption: O <sub>ot</sub> +O <sub>ot</sub> →O <sub>2</sub>	168 <sup>30</sup>	167	172
P <sub>6</sub> : Desorption: O <sub>br</sub> +O <sub>br</sub> →O <sub>2</sub>	414 <sup>30</sup>	450	465
P <sub>7</sub> : Desorption: O <sub>ot</sub> +O <sub>br</sub> →O <sub>2</sub>	291	308	318
P <sub>8</sub> : Desorption: CO <sub>ot</sub>	129 <sup>29</sup>	126	127
P <sub>9</sub> : Desorption: CO <sub>br</sub>	193 <sup>39</sup>	163	178
P <sub>10</sub> : Diffusion O <sub>ot</sub> →O <sub>ot</sub> :	106 <sup>30,40</sup>	154	148
P <sub>11</sub> : Diffusion O <sub>ot</sub> →O <sub>br</sub>	68 <sup>37</sup>	96	96
P <sub>12</sub> : Diffusion O <sub>br</sub> →O <sub>ot</sub>	191	238	243
P <sub>13</sub> : Diffusion O <sub>br</sub> →O <sub>br</sub>	87 <sup>30</sup>	164	151
P <sub>14</sub> : Diffusion CO <sub>ot</sub> →CO <sub>ot</sub>	106 <sup>29,40</sup>	125	125
P <sub>15</sub> : Diffusion CO <sub>ot</sub> →CO <sub>br</sub>	58 <sup>29</sup>	87	87
P <sub>16</sub> : Diffusion CO <sub>br</sub> →CO <sub>ot</sub>	122 <sup>29</sup>	124	143
P <sub>17</sub> : Diffusion CO <sub>br</sub> →CO <sub>br</sub>	87 <sup>41</sup>	87	90

P <sub>18</sub> : Recombination CO <sub>ot</sub> +O <sub>ot</sub>	89 <sup>42</sup>	75	69
P <sub>19</sub> : Recombination CO <sub>br</sub> +O <sub>br</sub>	133 <sup>42</sup>	142	135
P <sub>20</sub> : Recombination CO <sub>br</sub> +O <sub>ot</sub>	91 <sup>42</sup>	59	58
P <sub>21</sub> : Recombination CO <sub>ot</sub> +O <sub>br</sub>	89 <sup>42</sup>	96	71

From **Table 1**, it is evident that not a single rate-determining elementary step governs the reaction, but rather seven elementary steps reveal similar activation energies of 70-90 kJ/mol. In addition to these parameters the experimentally determined CO<sub>ot</sub>-CO<sub>ot</sub> repulsion of 10.6 kJ/mol was included in the kMC simulation. This value was determined by fitting the peak splitting of the CO<sub>ot</sub> desorption signal.<sup>21</sup> The CO<sub>ot</sub>-CO<sub>ot</sub> repulsion directly affects the desorption of CO<sub>ot</sub>, but also the recombination reactions of CO<sub>ot</sub> with undercoordinated surface O species (Brønsted-Evans-Polanyi (BEP) relation).<sup>43, 44</sup> In fitting the experimental TPR data, a factor 0.45 is determined for the corresponding BEP relations.

The differences between our experimentally determined activation barriers and the DFT-derived barriers by Seitsonen and Kiejna are within the generally accepted uncertainty of 20-30 kJ/mol for DFT calculations on the GGA level. These deviations can be traced back to the fact that our experiment-based values were determined as ‘effective (averaged) parameters’ by fitting the CO<sub>2</sub> thermal desorption signals from surface science experiments. These energies do not directly correspond to the DFT-calculated values which are valid only for the single configuration that was used to model the transition state (without averaging over various surface configurations). Therefore, a direct comparison between the DFT-based and experiment-based values is misleading.

With this experiment-based kMC approach, both the experimental kinetic reaction data and the infrared spectroscopy data under steady state flow conditions in the 10<sup>-7</sup> mbar range can be rationalized (cf. Fig. 2). The experiment-based kMC simulations retrieve an apparent activation energy of 79 kJ/mol for a reaction mixture consisting of  $p(\text{CO}) = 3 \cdot 10^{-7}$  mbar and  $p(\text{O}_2) = 1 \cdot 10^{-7}$  mbar. KMC simulations based on this very same parameter set of activation energies reproduce equally well the experimental Arrhenius plot for  $p(\text{CO}) = 10$  mbar and  $p(\text{O}_2) = 5.5$  mbar for temperatures up to 550 K, disclosing an apparent activation energy of 77 kJ/mol.<sup>45</sup>

The quantitative agreement of experimental (about 80 kJ/mol) and kMC simulated apparent activation energies demonstrates that the intricate interplay of elementary reaction steps with similar activation energies in the range of 80-120 kJ/mol is properly accounted for. However, we have to emphasize that the experiment-based kMC simulations include a

pairwise repulsion among the adsorbed  $\text{CO}_{\text{ot}}$  molecules of 10.6 kJ/mol which is decisive in obtaining the correct apparent activation energy for the CO oxidation over  $\text{RuO}_2(110)$ . Neglecting lateral repulsion between  $\text{CO}_{\text{ot}}$  molecules, the surface will be fully covered by CO, making dissociative adsorption of  $\text{O}_2$  impossible. Thus, the overall reaction rate will be determined by the desorption of two neighboring  $\text{CO}_{\text{ot}}$  molecules, leading to an apparent activation energy of 260-280 kJ/mol.

In Fig. 2a we summarize the kMC results of the turnover frequency (TOF) as a function of the reactant feed ratio  $p(\text{CO})/p(\text{O}_2)$ , while keeping the partial pressure of oxygen constant at  $10^{-7}$  mbar and the sample temperature at 350 K. Near the optimum reaction conditions of  $p(\text{CO})/p(\text{O}_2) = 2$ , the simulated TOF values are by a factor of 2.5 larger than the experimental TOF values. However, the variation of the TOF dependent on the reactant feed ratio is well reproduced. This deviation is within an acceptable magnitude, considering the various approximations employed when comparing the experimental with the simulated data. For a more detailed discussion on the origin of this deviation, refer to section 4 or Ref. 21.

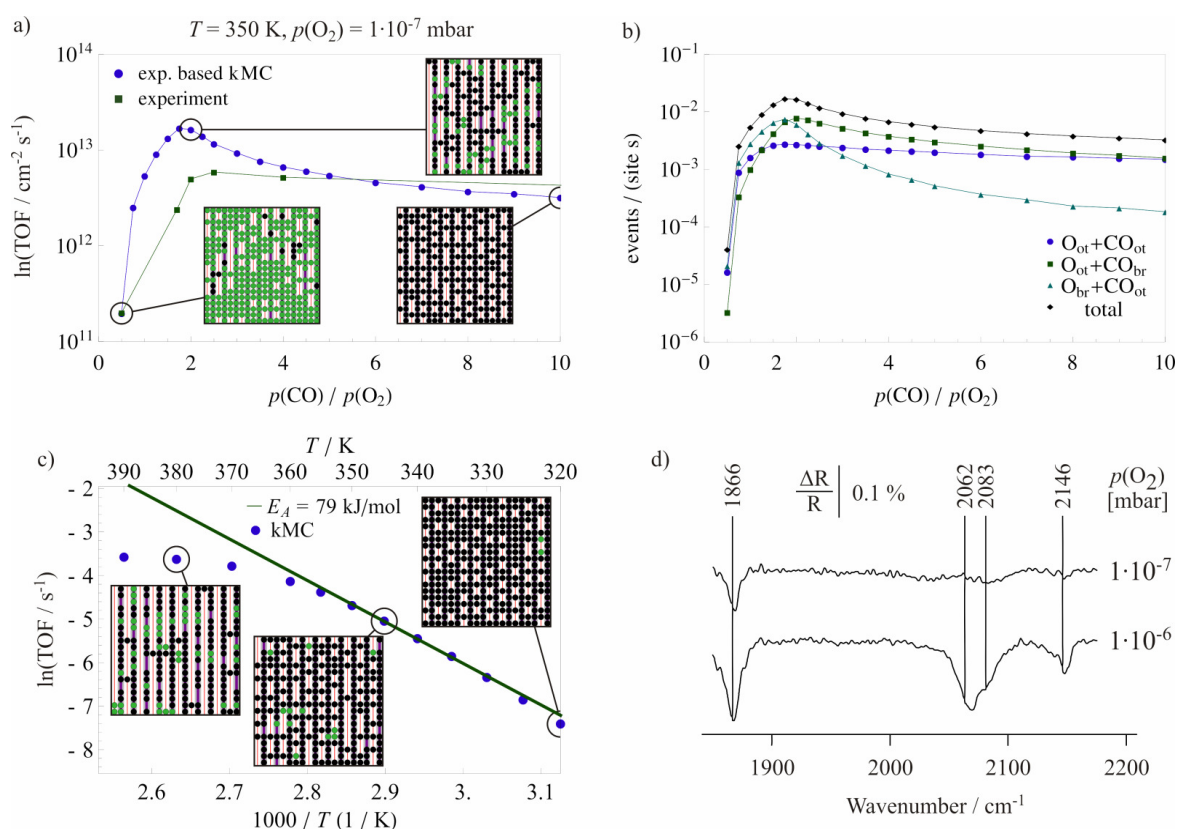


**Fig. 2:** Oxidation of CO over  $\text{RuO}_2(110)$  at 350 K with constant  $p(\text{O}_2) = 10^{-7}$  mbar. **a)** TOF as a function of the reactant feed ratio  $p(\text{CO})/p(\text{O}_2)$ : kMC simulation (circles) and experimental values<sup>28</sup> (squares). Insets show the kMC simulated spatial distributions of reactants at the surface for three different feed ratios  $p(\text{CO})/p(\text{O}_2) = 0.5, 2, 10$ . Color code: O (green), CO (black), vacant 1f-cus Ru sites (red stripes), vacant 2f-cus Ru sites (purple stripes). **b)** Contributions of the elementary O + CO recombination steps ( $\text{O}_{\text{ot}} + \text{CO}_{\text{ot}}$ ,  $\text{O}_{\text{ot}} + \text{CO}_{\text{br}}$ , and  $\text{O}_{\text{br}} + \text{CO}_{\text{ot}}$ ) to the total TOF. Due to the high activation barrier for  $\text{O}_{\text{br}} + \text{CO}_{\text{br}}$ , this elementary step does not contribute significantly to the overall rate at 350 K and is

therefore not shown here. **c)** Oxidation of CO over RuO<sub>2</sub>(110) in the 320-390 K temperature range at constant partial pressures  $p(\text{O}_2) = 1 \cdot 10^{-7}$  mbar and  $p(\text{CO}) = 3 \cdot 10^{-7}$  mbar. Arrhenius plot of the kMC simulated TOF values, indicating an apparent activation energy of 79 kJ/mol in the 320-360 K range. Snapshots of the kMC-simulated surface configurations are shown for selected temperatures. **d)** Experimental RAIR spectra in the C-O bond stretching range, recorded during the oxidation of CO over RuO<sub>2</sub>(110) at 350 K with  $p(\text{O}_2) = \frac{1}{2} p(\text{CO}) = 10^{-7}$  and  $10^{-6}$  mbar<sup>45</sup>.

For three typical reaction conditions  $p(\text{CO})/p(\text{O}_2) = 0.5, 2, 10$  the surface configurations are shown as snapshots of the kMC simulations after reaching steady state conditions (cf. Fig. 2a insets). At optimum reaction conditions with highest TOF ( $p(\text{CO})/p(\text{O}_2) \approx 2$ ), most of the bridging O atoms are replaced by CO and the rest of the 2f-cus Ru sites are vacant or occupied by bridging O. The 1f-cus Ru sites are mostly vacant and only a few sites are occupied by on-top CO, indicating that most of the on-top CO molecules react easily with oxygen to form CO<sub>2</sub>. For oxidizing reaction conditions ( $p(\text{CO})/p(\text{O}_2) = 0.5$ ), the surface is mainly covered by bridging O and on-top O. The few CO molecules found on the surface reside mostly in bridge position. CO molecules which adsorb in the vacant on-top positions readily recombine with neighboring O, thus explaining the remaining activity of this surface and the absence of on-top CO in the kMC snapshot. Under strongly reducing reaction conditions ( $p(\text{CO})/p(\text{O}_2) = 10$ ), the 2f-cus Ru sites are almost exclusively occupied by bridging CO. About 50 % of the 1f-cus-Ru sites are populated by CO, while the other half remains vacant, thereby forming an approximately ordered (1 × 2) adsorbate layer of CO<sub>ot</sub>. The incomplete coverage of on-top CO - despite the strongly reducing gas mixture - is due to the maximum in CO<sub>ot</sub> desorption at 320 K and to the small CO partial pressure of 10<sup>-7</sup> mbar. This surface is not poisoned by CO but rather is quite active, as also experimentally observed. Between neighboring on-top CO there are several vacant 1f-cus sites onto which molecular oxygen can readily adsorb dissociatively. Subsequently, on-top O and on-top CO recombine rapidly to form CO<sub>2</sub>, so that in the kMC snapshot no on-top O is visible. From the snapshots in Fig. 2a it becomes clear that the 1-dimensional character of the RuO<sub>2</sub>(110) has largely been lost in the CO oxidation reaction since both 1f-cus Ru and 2f-cus Ru sites are substantially involved in the surface reaction.

The great benefit of kMC simulations is that the overall TOF can be decomposed into the contributions of the relevant elementary recombination steps. This information is not readily available by experiments. In Fig. 2b the contributions of the three leading elementary recombination steps (O<sub>ot</sub> + CO<sub>ot</sub>, O<sub>ot</sub> + CO<sub>br</sub>, and O<sub>br</sub> + CO<sub>ot</sub>) as a function of the composition of the reaction mixture are detailed. Under oxidizing reaction conditions the main contributions to the TOF come from the recombination of on-top CO with both bridging O

and on-top O, while under strongly reducing conditions the recombination of on-top O with both bridging CO and on-top CO determines the TOF. For the optimum reaction mixture  $p(\text{CO})/p(\text{O}_2) \approx 2$  all three recombination steps are equally important for the CO oxidation reaction. These kMC simulations disclose an important property of the reaction system in that the rate determining reaction step changes with the reaction conditions.

The temperature dependence of the activity can be simulated in kMC by setting different temperature values while keeping  $p(\text{CO}) = 3 \cdot 10^{-7}$  mbar and  $p(\text{O}_2) = 10^{-7}$  mbar fixed. The kMC simulated activity data are summarized in Fig. 2c in the form of an Arrhenius plot. Between 320 K and 360 K the  $\ln(\text{TOF})$  decreases linearly with  $1/T$ . The corresponding apparent activation energy of 79 kJ/mol is close to the value of 82 kJ/mol found in experiments.<sup>46</sup> From snapshots of the spatial distribution of reactants on the surface (cf. insets of Fig. 2c) the surface configuration related to the kinetic branch of the Arrhenius plot is dominated by adsorbed CO. At 345 K the bridge positions are occupied by CO, while about half of the 1f-cus sites are vacant and the rest is mostly occupied by on-top CO; only few on-top O atoms are visible in this snapshot. In the bend-over region of the Arrhenius plot above 380 K, the bridge sites of RuO<sub>2</sub>(110) are occupied by both CO and oxygen, while the 1f-cus sites are mostly vacant. For low temperatures around 320 K, all bridge sites are occupied by CO and about 60% of the 1f-cus sites are occupied by CO; only rarely on-top O is seen.

In a recent series of RAIRS experiments<sup>45</sup> the CO oxidation reaction over RuO<sub>2</sub>(110) was studied *in situ* at a constant temperature of 350 K under the stoichiometric reaction mixture  $p(\text{CO})/p(\text{O}_2) = 2$  and varying oxygen partial pressure from  $10^{-7}$  to  $10^{-6}$  mbar (cf. Fig. 2d). Since the observed CO stretching frequency depends sensitively on the local environment, the RAIR spectra have been shown to provide unprecedented information about the distribution of the reactants on the surface which can directly be compared with configurations determined by kMC. This approach represents probably the most direct and reliable way to assess the quality of kMC simulations.<sup>21, 45</sup>

At  $p(\text{O}_2) = 10^{-7}$  mbar, the IR spectrum reveals only one vibrational band at  $1866 \text{ cm}^{-1}$  which is unambiguously assigned to bridging CO sparsely populating the 2f-cus-Ru sites with no on-top CO on 1f-cus sites in the direct neighborhood. By increasing the partial pressure of oxygen to  $10^{-6}$  mbar while keeping the stoichiometry of the reactant feed, an on-top CO species is identified in addition to the bridging CO, both residing in domains with a high local CO coverage. These domains characterized by the two vibrational bands at  $2062 \text{ cm}^{-1}$  and  $2083 \text{ cm}^{-1}$  are stable under reaction conditions because the high local CO coverage precludes dissociative adsorption of O<sub>2</sub> into these domains and therefore the removal of CO by CO-O

recombination. At the same time the emergence of areas predominantly covered by O in both on-top and bridging positions can be observed in RAIRS. The CO molecules which adsorb into vacancies within these O-covered domains lead to the vibrational band at  $2146\text{ cm}^{-1}$ , as observed in Fig. 3. These spectroscopic details on the surface configuration are fully reconciled with the experiment-based kMC simulations (see snapshot in Fig. 2a for stoichiometric reaction mixture).

### 3.2.3 DFT-Based Kinetic Monte Carlo Simulations

A straightforward step forward in theoretical catalysis is to couple standard kMC simulations with ab-initio calculations as suggested by Fichthorn und Weinberg<sup>47</sup> and first realized by Hansen and Neurock.<sup>48</sup>

In the following we compare the results of DFT-based kMC simulations using two different parameter sets.<sup>49</sup> In **Table 1** we listed the energy barriers of these parameter sets as derived from DFT calculations. The Kiejna data set uses the full-potential method (FP-LAPW)<sup>35</sup> method (Wien2k code<sup>50,51</sup>). The second parameter set<sup>36</sup> (*Seitsonen*) was calculated with the VASP code<sup>52</sup> using pseudopotentials.<sup>53</sup> Both studies used the same type of generalised gradient approximation for the exchange-correlation functional PBE.<sup>54</sup>

The activation energies for desorption and recombination (cf. **Table 1**) of the two ab-initio calculations are within a generic uncertainty estimate of 20-30 kJ/mol.<sup>43, 55</sup> However, the energy barriers of both ab-initio parameter sets exhibit a different ordering in that the recombination of  $\text{O}_{\text{ot}}+\text{CO}_{\text{ot}}$ ,  $\text{O}_{\text{ot}}+\text{CO}_{\text{br}}$ , and  $\text{O}_{\text{br}}+\text{CO}_{\text{ot}}$  are virtually identical in the *Seitsonen* set, while in Kiejna's parameter set, the recombination with the lowest activation energy is  $\text{O}_{\text{ot}}+\text{CO}_{\text{br}}$ , followed by  $\text{O}_{\text{ot}}+\text{CO}_{\text{ot}}$ , and  $\text{O}_{\text{br}}+\text{CO}_{\text{ot}}$ . The reason for this discrepancy has been traced back to different geometries in the transition state. A more detailed discussion can be found in Refs. 36, 46, and 49. The values of the activation energy of diffusion in the *Kiejna* set were adapted from the parameter set of Reuter.<sup>41</sup>

In Fig. 3a, b we compare the kMC simulated TOF values and their decomposition into the elementary reaction steps for the two parameter sets, plotted as a function of the reactant feed ratio  $p(\text{CO})/p(\text{O}_2)$  for  $T = 350\text{ K}$  and  $p(\text{O}_2) = 10^{-7}\text{ mbar}$ . Both parameter sets lead to remarkably similar results for reducing conditions. However, the discrepancies are substantial for oxidizing reaction conditions. In comparison with experimental TOF values the maximum TOF is about 3 times higher than in the actual experiments but the optimum reactant feed agrees well with the experimental one, and poisoning of the  $\text{RuO}_2(110)$  catalyst occurs most notably for strongly oxidizing reaction conditions with  $p(\text{CO})/p(\text{O}_2) < 1$ . Under optimum

reaction conditions all three elementary reaction steps contribute equally to the overall TOF, while under reducing reaction conditions the recombination of on-top O with bridging CO prevails for both parameter sets and the  $\text{CO}_{\text{ot}} + \text{O}_{\text{br}}$  process is negligible since almost all bridging O are replaced by CO. For more oxidizing reaction conditions, inhibition sets in quite abruptly and the most relevant reaction step critically depends on the chosen parameter set. With Seitsonen's parameter set  $\text{O}_{\text{br}} + \text{CO}_{\text{ot}}$  and  $\text{O}_{\text{ot}} + \text{CO}_{\text{ot}}$  are equally important for the residual activity, while with Kiejna's parameter set only the  $\text{O}_{\text{ot}} + \text{CO}_{\text{ot}}$  recombination dominates the activity.

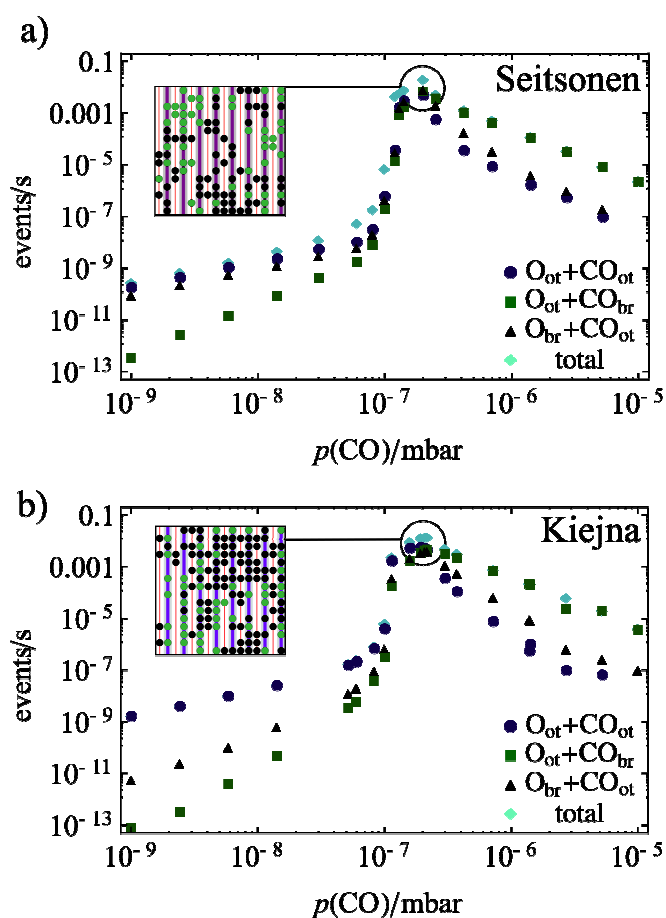


**Fig. 3:** Contributions of each elementary O+CO recombination step ( $\text{O}_{\text{ot}} + \text{CO}_{\text{ot}}$ ,  $\text{O}_{\text{ot}} + \text{CO}_{\text{br}}$ ,  $\text{O}_{\text{br}} + \text{CO}_{\text{ot}}$ ) to the total TOF for  $p(\text{O}_2) = 10^{-7}$  mbar and variable CO partial pressure at 350 K, simulated with the parameters sets of Kiejna (a) and Seitsonen (b). Due to the high activation barriers for  $\text{O}_{\text{br}} + \text{CO}_{\text{br}}$ , this elementary step does not contribute significantly to the overall rate at 350 K and is not shown here. The snapshot of a kMC generated steady-state configuration under optimum reaction conditions at  $T = 350$  K and  $p(\text{O}_2) = 10^{-7}$  mbar according to c) the parameter set of Kiejna ( $p(\text{CO}) = 2.5 \cdot 10^{-7}$  mbar) and to d) the parameter set of Seitsonen ( $p(\text{CO}) = 2 \cdot 10^{-7}$  mbar).

KMC simulated snapshots of the distribution of reactants (CO and O) on  $\text{RuO}_2(110)$  under optimum reaction conditions are shown in Fig. 3a,b. In the kMC snapshot of Seitsonen,

the 2f-cus Ru sites are partially occupied by bridging CO while most of 2f-cus Ru sites are either vacant or occupied by oxygen. In the kMC snapshot of Kiejna most the bridge site are occupied by O and CO; only few vacancies are observed. In both kMC snapshots, we can recognize small domains of densely packed CO and densely packed O. This kind of kinetic phase separation has first been described theoretically in the seminal paper of Ziff, Gulari and Barshad.<sup>56</sup> This 'phase separation' is also evident from RAIRS experiments.<sup>45</sup>

From an experimental point of view, Arrhenius plots comprise the standard methods to characterize a catalyzed reaction system in terms of an apparent activation energy. Typical values for the apparent activation energies of the catalyzed CO oxidation over RuO<sub>2</sub>(110) lie in the range of 60-80 kJ/mol.<sup>28, 46, 57, 58</sup> Surprisingly, DFT-based kMC leads to apparent activation energies of 270 kJ/mol for the parameter sets presented herein (data not shown) which even exceed that of the homogeneous gas phase reaction, thus being considered to be unreliable. The main reason for this obvious discrepancy lies in the missing lateral interaction among the reaction intermediates on the surface in the DFT-based kMC.<sup>49</sup> While an extensive review on the possible methods to determine these values from DFT calculations is outside the scope of this perspective, the reader is referred to Ref. 13 for an introduction on the determination of lateral interactions from DFT calculations. For the interaction between O<sub>ot</sub> and O<sub>br</sub> species, pairwise interactions are available from Ref. 33. Although these parameters would substantially improve the kMC model for the CO oxidation on RuO<sub>2</sub>(110), they were not included in the present study to ensure internal consistency of the parameter sets.

Concluding this comparison, experimental TOF values plotted as a function of the reactant feed ratio do not provide a criterion which is able to discriminate between the sets of energy barriers of Kiejna and Seitsonen. This is quite surprising, as from the activation energies of the recombination of CO with O one would have anticipated that the changed relevance of the elementary reaction steps will inevitably lead to different reaction kinetics. This observation manifests impressively the fundamental problem of chemical kinetics, namely that a proposed reaction mechanism can only be ruled out but never be properly proven on the basis of purely kinetic data.<sup>1</sup> Instead of the simple kinetic reaction data, the configuration of reactants on the catalyst's surface could serve as a benchmark when comparing ab-initio kMC results to experiment. In this way RAIRS was able to differentiate between the parameter set proposed by Reuter<sup>32</sup> and that of Seitsonen/Kiejna.<sup>35,36,49</sup> However, for the parameter sets of Kiejna and Seitsonen this comparison with RAIRS is not conclusive as indicated in Fig. 3a,b. Despite the difference in overall coverage, the configurations of the

reaction intermediates are quite similar. Therefore, the transformation of such snapshots into RAIRS spectra, as reported in a recent paper <sup>21</sup>, will result in similar spectra, and is thus not able to differentiate between both parameter sets. To resolve this problem of differentiation among different parameter sets, one needs to simulate the reaction under various reaction conditions to identify reaction conditions where both parameter sets will lead to substantial differences either in the overall kinetics or in the surface configuration.

Such a desired situation is encountered for a reaction temperature of 325 K, where desorption of CO is largely suppressed. The steady state surface configurations for stoichiometric reaction conditions is identical for kMC simulation using Kiejna's and Seitsonen's parameter set. However, in the transient region starting from a stoichiometric RuO<sub>2</sub>(110) surface and exposing the surface to  $p(\text{CO}) = 2 \cdot 10^{-7}$  mbar and  $p(\text{O}_2) = 10^{-7}$  mbar both parameter sets lead to distinctly different surface configurations as shown in Fig. 4 and by movies provided on our web site.<sup>59</sup> With Seitsonen's parameter set, densely packed CO domains evolve where both the bridge and the on-top sites are occupied by CO (would lead to a vibration of 2060cm<sup>-1</sup> in RAIRS). Quite in contrast, kMC simulations with the Kiejna data set indicate that first the 1f-cus sites are saturated by on-top CO (RAIRS: vibration at 2000cm<sup>-1</sup>) and slowly the bridging O are replaced by CO keeping the 1f-cus sites occupied by CO. Since the transient region expands over several 100 s, RAIRS experiments should be able to readily discriminate between these two situations.

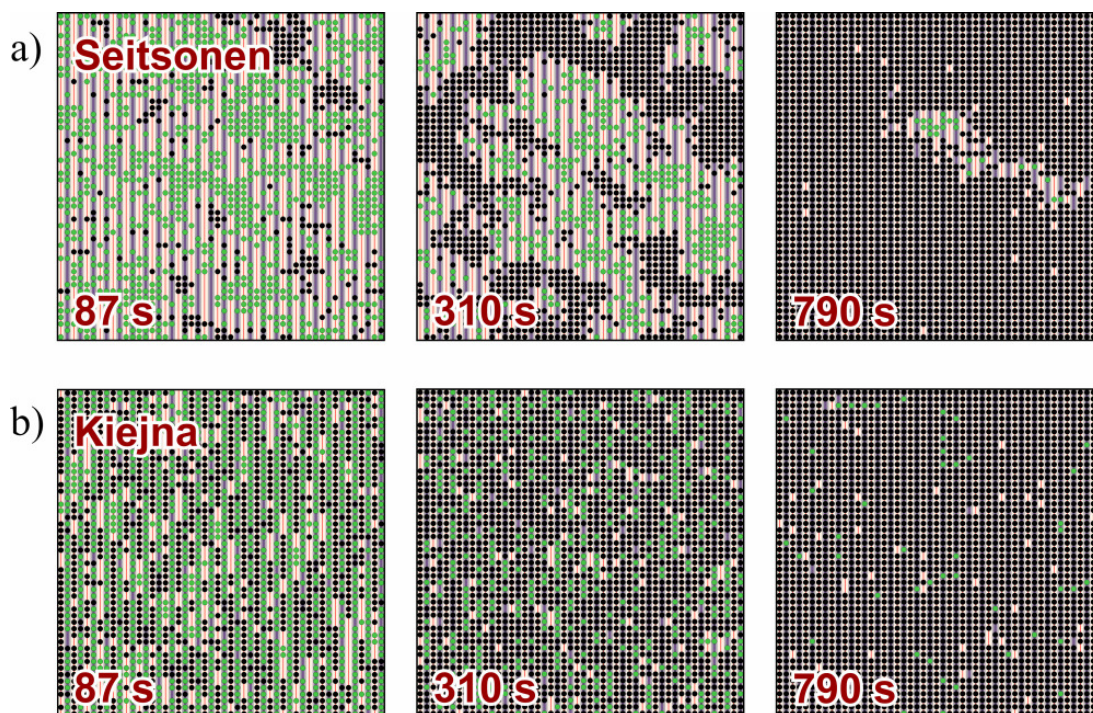


**Fig. 4:** Time evolution (87 s, 310 s, 790 s) of the kMC-simulated configurations with time in the transient region starting from a stoichiometric RuO<sub>2</sub>(110) surface and exposing the surface to  $p(\text{CO}) = 2 \cdot 10^{-7}$  mbar and  $p(\text{O}_2) = 10^{-7}$  mbar at  $T = 325$  K. KMC simulations using

the parameter set of Seitsonen (a) and Kiejna (b). Both parameter sets lead to a fully CO poisoned surface at steady state, but during the induction period, the surface configurations are distinctly different.

### 3.2.4 Comparison: Mean Field Approach versus Kinetic Monte Carlo Simulations in Microkinetic Modeling

Mean field (MF) based microkinetic modeling has been applied extensively to analyze chemical kinetics in heterogeneously catalyzed reactions on single-crystal surface studied under low pressure conditions.<sup>9</sup> While such analyses have been particularly instructive, their limitations are long-recognized.<sup>8</sup> The mean field assumption of well-stirred spatially randomized reactants generally may break down for instance due to adlayer ordering or islanding. Of course, these limitations can be overcome by development of realistic atomistic lattice gas models which can be analyzed by kMC simulations.

Only recently, the different outcomes of simulations have been quantified by direct comparison of kMC and MF methods applied to the very same reaction system, namely the CO oxidation at RuO<sub>2</sub>(110).<sup>60, 61</sup> It turned out that TOF values determined by these methods can easily deviate by several orders of magnitude for oxidizing conditions due to strong site correlations, inclining the authors to conclude that MF-based microkinetic modeling is only of limited value. However, these studies are based on a parameter set of activation and adsorption energies which ignores the interaction among the reactants on the surface.

Since strong site correlations are sensitively affected by lateral interactions, we critically compared MF and kMC based methods in the microkinetic modeling of the CO oxidation at RuO<sub>2</sub>(110) explicitly including lateral interaction.<sup>62</sup> To simplify the comparison with the data previously published by Reuter and coworkers, the original parameter set by Reuter<sup>41</sup> was applied, including however a weak lateral repulsion of up to 14.4 kJ/mol between neighboring O<sub>ot</sub> atoms. This value is justified by DFT calculations previously published by Wang and Schneider.<sup>33</sup>

The results of our kMC simulations for  $T = 510$  K and  $p(\text{O}_2) = 5.5$  mbar are summarized in Fig. 5a. The red curve (no repulsion) shows a similar dependency on  $p(\text{CO})$  as previously published by Temel et al.<sup>60</sup> The maximum activity can be found at  $p(\text{CO}) \approx 11$  mbar. If  $p(\text{CO})$  is slightly lowered (oxidizing regime), the TOF drops sharply by 4 orders of magnitude and continues to decrease steadily. The sharp decline in TOF can be explained by pair correlation: each time a CO<sub>2</sub> molecule is formed, a pair of neighboring vacancies is formed on the surface (see Fig. 5c, I). At oxidizing conditions, the impingement rate of O<sub>2</sub> is higher than

that of CO, so the pair of vacancies will be filled via dissociative adsorption of O<sub>2</sub> in most cases. The result is a surface that is entirely covered by oxygen atoms and no CO molecules can adsorb. In this situation, the recombination of two neighboring O<sub>ot</sub> to form O<sub>2</sub> becomes the rate limiting step. Since the activation energy for this step is 193 kJ/mol, the overall TOF is 4 orders of magnitude lower than at the maximum of reactivity, where the recombination of O<sub>ot</sub> with CO<sub>ot</sub> (86 kJ/mol) is rate limiting.

What happens if a weak lateral repulsion between next neighboring O<sub>ot</sub> is included into the model while keeping all other parameters constant? Again, whenever a CO<sub>2</sub> molecule is formed, a pair of vacancies is left behind. However, due to the repulsion, there is a driving force to increase the distance between O<sub>ot</sub>, resulting in a decrease of the diffusion barrier, as schematically depicted in Fig. 5c, III. As a result, the pair of vacancies turns into two single vacancies, separated by a single O<sub>ot</sub>. For single vacancies, the preferred process is adsorption of a CO molecule, so that the formation CO<sub>2</sub> is again possible. This leads to an increase in TOF under oxidizing conditions due to the lateral O<sub>ot</sub>-O<sub>ot</sub> repulsion (cf. Fig. 5a). At the highest repulsion used in this study (14.4 kJ/mol), the TOF at oxidizing conditions is only about a factor of 20 lower than at optimum conditions. The increased activity is accompanied by a shift of the maximum activity to  $p(\text{CO}) \approx 6$  mbar.

With microkinetic modeling based on the mean-field approach (MFA) in the absence of lateral interactions, (Fig. 5b, red curve), the overall trend is quite similar to the kMC simulations in that the maximum of reactivity is found at  $p(\text{CO}) \approx 15$  mbar and the TOF drops as  $p(\text{CO})$  is reduced. However, the drop is significantly less pronounced than in kMC (with zero repulsion). The higher rate of MFA can be traced back to the fundamental difference between MF and kMC (cf. Fig. 5c, II): Under oxidizing conditions, adsorption of O<sub>2</sub> can take place in kMC if a pair of adjacent vacancies exists on the surface. As explained above, this results in total poisoning of the surface with O in the absence of repulsion. In MF on the other hand, the adsorption rate of O<sub>2</sub>,  $r_{\text{ads}}(\text{O}_2)$  is proportional to  $\theta^{*2}$  with  $\theta^* = (1 - \theta_{\text{total}})$ , while the adsorption rate of CO,  $r_{\text{ads}}(\text{CO})$  is proportional to  $\theta^*$ . Accordingly, at high total coverage  $\theta_{\text{total}}$ ,  $r_{\text{ads}}(\text{CO})$  is in general higher than  $r_{\text{ads}}(\text{O}_2)$ . As a result, total poisoning with O is avoided in MFA and the surface remains active, even under oxidizing conditions.

Although the effect of pair correlation discussed above does not emerge in the mean-field approach (MFA), the effect of lateral repulsion can also be studied within this framework (cf. Fig. 5c). The inclusion of lateral repulsion leads to an increase in TOF under oxidizing conditions, similar to the results obtained in kMC. In the MFA, the increase in TOF can be traced back to the reduction of O<sub>ot</sub> coverage due to lateral repulsion, facilitating the

adsorption of CO and subsequent reaction to CO<sub>2</sub>. At a repulsion of 14.4 kJ/mol, the maximum of activity can be found at  $p(\text{CO}) \approx 6$  mbar. The TOF is still overestimated by a factor of 5 if compared to kMC. Since MFA uses a uniform distribution of adparticles, the effect of repulsion is somewhat overestimated while the effect of attraction is underestimated. To achieve perfect agreement with kMC, a more accurate model to treat the pairwise repulsion like the quasi-chemical approximation (QCA) is required.<sup>63</sup>

At a maximum repulsion of 14.4 kJ/mol, MF and kMC derived TOFs under oxidizing conditions differ only by a factor of 5, compared to almost 4 orders of magnitude without repulsion. The CO partial pressure at which the reactivity is maximized was slightly higher in MF than in kMC without lateral interactions but was quantitatively reproduced at maximum lateral interactions. These results reveal that kMC is, as expected, very sensitive to factors that control the distribution of the adparticles on the surface. Without lateral repulsion, spatial effects like the pair correlation govern the catalyst activity. However, such effects vanish to a large extent if a more realistic model is applied that includes lateral interactions. MFA, on the other hand, is not as sensitive to the interactions as kMC because it does not take into account the spatial distribution of adparticles on the surface. It works best when the particles are perfectly mixed and worst when reactants are separated on the surface, or spatial correlation completely prevents the adsorption of one or more species. However, in general, industrially relevant reactions take place at conditions with highest activity, just at those temperatures where the Arrhenius plot starts to bend over. Under these conditions, the adsorbed reactants and fragments are well intermixed at the surface so that MF is a sufficiently precise approach to model the microkinetics of this reaction.

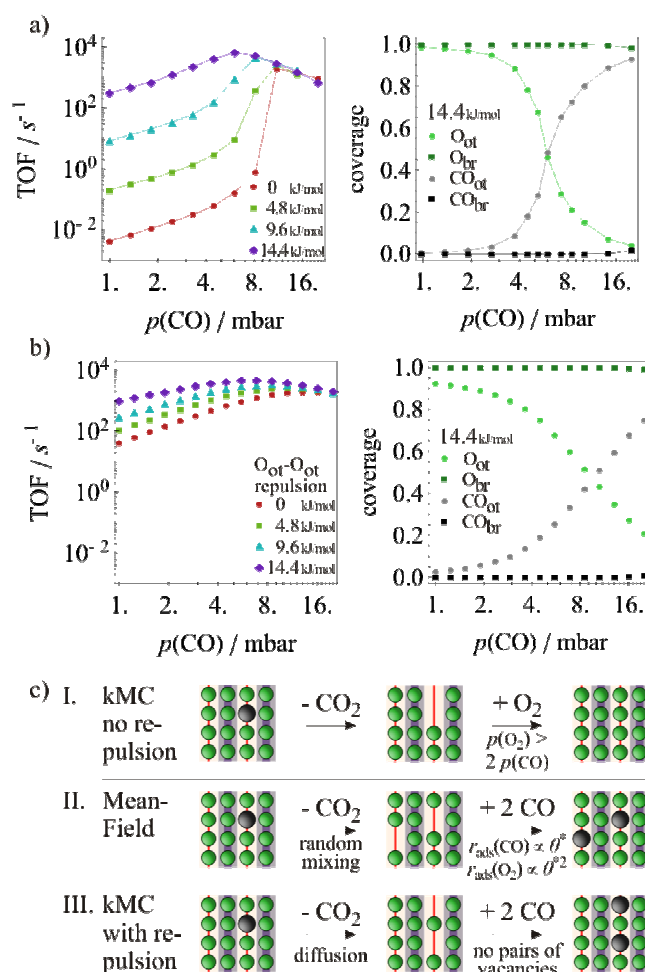


**Fig. 5:** Comparison between Mean-Field-Approach (MFA) and kMC for the oxidation of CO over RuO<sub>2</sub>(110) at  $T = 510$  K and  $p(\text{O}_2) = 5.5$  mbar. The O<sub>ot</sub>-O<sub>ot</sub> repulsion was varied between 0 and 14.4 kJ/mol. Coverages are shown only for the 14.4 kJ/mol case. a) TOFs (left) and coverages (right) for kMC simulations, b) TOFs (left) and coverages (right) for MFA calculations, c) The most likely scenarios under oxidizing conditions for the three modeling approaches. After formation of a CO<sub>2</sub> molecule, the O<sub>ot</sub> overlayer reorders in different ways, depending on the modeling approach. This leads to **I.** complete poisoning of the surface with O<sub>ot</sub> in kMC without repulsion, **II.** Sustained activity because CO adsorption happens faster than O<sub>2</sub> adsorption for a random distribution of adparticles in the MFA, and **III.** Sustained activity because pair correlation of vacancies is lifted due to repulsive interaction, preventing poisoning by dissociative O<sub>2</sub> adsorption in kMC simulations.

The present comparison between MF and kMC based methods demonstrates that kMC simulations can easily lead to a wrong estimation of the TOF by 4 orders of magnitude when lateral interaction of surface intermediates are neglected. With a more realistic model for both kMC and MFA, where lateral interactions are properly included, almost perfect agreement between the two methods is accomplished for the CO oxidation over RuO<sub>2</sub>(110).

### 3.3 HCl oxidation at RuO<sub>2</sub>(110)

#### 3.3.1 Molecular insight into the HCl oxidation over RuO<sub>2</sub>(110)

Most of the molecules from the gas phase enter the RuO<sub>2</sub>(110) surface via the 1f-cus Ru sites<sup>25</sup>, while the dehydrogenation of molecules proceeds via a hydrogen transfer to undercoordinated surface O atoms such as O<sub>br</sub> and O<sub>ot</sub>.<sup>24</sup> Upon exposure to HCl molecules at temperatures above 500 K, the stoichiometric RuO<sub>2</sub>(110) surface is transformed into a chlorinated surface where the bridging O atoms are partially replaced by chlorine.<sup>64-66</sup>

The surface reaction of HCl oxidation over surface chlorinated RuO<sub>2</sub>(110) is summarized by the catalytic cycle depicted in Fig. 6. All elementary reaction steps are confined along the 1-dimensional rows of 1f-cus Ru sites and no communication between the 1f-cus Ru rows across the O<sub>br</sub> rows except hydrogen transfer takes place, rendering this a 1-dimensional catalyst. Both O<sub>2</sub> and HCl adsorb dissociatively on the partly chlorinated RuO<sub>2</sub>(110) surface.<sup>67</sup> The adsorption energy of oxygen is 200 kJ/mol per pair.<sup>32, 33, 36</sup> The energy gain of the first (dissociative) HCl adsorption amounts to 125 kJ/mol. In this step, hydrogen from HCl is transferred to the O<sub>ot</sub> in a dissociative adsorption process, while Cl<sub>ot</sub> is bound atop to 1f-cus Ru. The second HCl molecule dissociates upon adsorption, transferring its H atom to the previously formed O<sub>ot</sub>H species, thereby producing water, O<sub>ot</sub>H<sub>2</sub>. The adsorption energy of the second HCl molecule is 175 kJ/mol. Water molecules are bound by 120 kJ/mol to the surface so that water desorption sets in at around 420 K.<sup>68, 69</sup>

The recombination process of neighboring Cl<sub>ot</sub> species to form molecular Cl<sub>2</sub> is activated by 228 kJ/mol and constitutes the elementary step with the highest activation barrier encountered in this catalytic cycle. Accordingly, the catalyst temperature must be at least 600 K to be able to liberate the desired product, chlorine, from the surface.<sup>64, 67, 70, 71</sup> Yet, from kinetic experiments the rate determining step has been proposed to be the dissociative adsorption of oxygen under typical reaction conditions, as corroborated by microkinetic modeling.<sup>23, 72</sup> The reason is that under typical reaction conditions the RuO<sub>2</sub>(110) surface is mostly covered by chlorine which is substantially more strongly bound than on-top oxygen. Therefore, oxygen adsorption, which requires two neighboring 1f-cus Ru sites, is inhibited.<sup>24</sup>

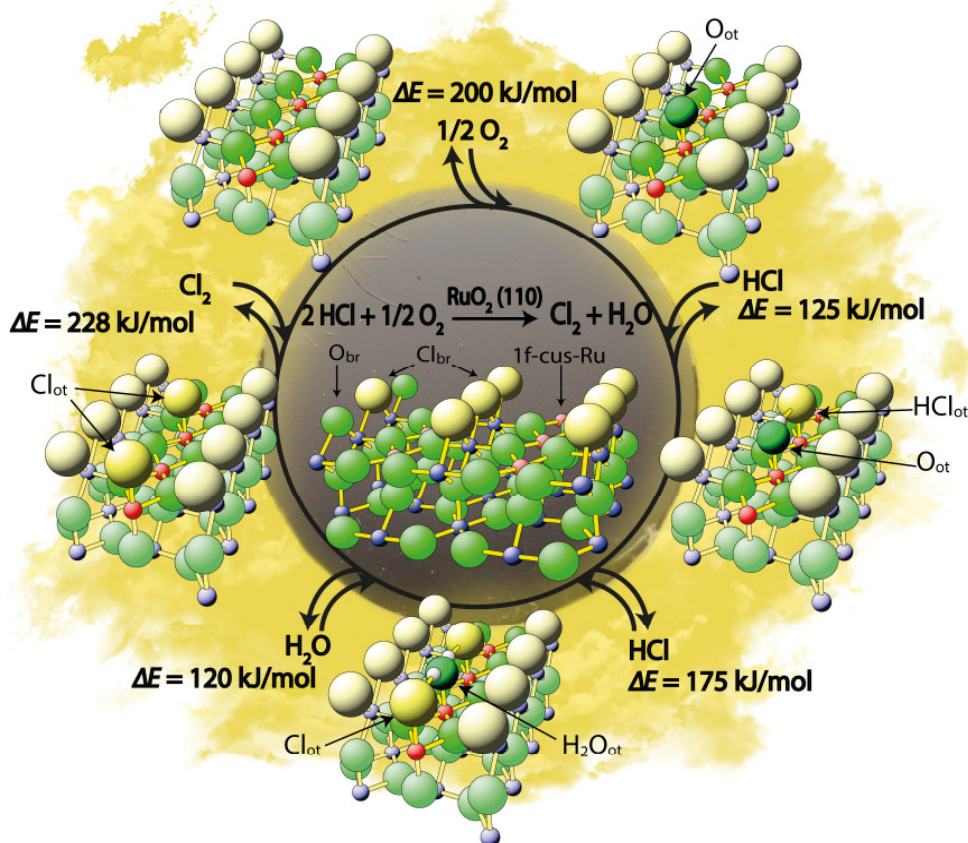


**Fig. 6:** Catalytic cycle of the HCl oxidation over chlorinated RuO<sub>2</sub>(110). In the schematic representation of RuO<sub>2</sub>(110) the green balls are the oxygen atoms and the blue/red balls are Ru atoms in bulk-environment and (undercoordinated) at the surface, respectively. The chlorine atoms are represented by large yellow balls. In the HCl oxidation reaction (Deacon process) over RuO<sub>2</sub>(110) both reactants O<sub>2</sub> and HCl adsorb dissociatively: Subsequently, surface oxygen is reduced to the by-product water by H coming from dissociative HCl adsorption. Water desorbs at around 420 K, and the remaining adsorbed chlorine atoms can recombine to form the desired product Cl<sub>2</sub> at temperatures around 600 K. All energies given were calculated by DFT.<sup>36, 67</sup>  $\Delta E$  defines the adsorption energies which determine the dynamical adsorption/desorption equilibrium between the surface and the gas phase. Copyright © 2012 American Chemical Society

The experimentally determined desorption temperatures of water, oxygen, HCl, Cl<sub>2</sub> are 420 K, 400 K, 550 K, and 600 K respectively.<sup>64, 67</sup> Since these desorption temperatures are only slightly lower than the actual reaction temperatures of about 600 K, the surface reactions are strongly coupled with gas phase via adsorption and desorption in the catalyzed HCl oxidation over RuO<sub>2</sub>(110).

In Fig. 6 this intimate interplay is pictorially emphasized by the yellow clouds around the model catalyst/catalytic cycle. For instance, readsorption of water inhibits the HCl oxidation reaction since water blocks active 1f-cus Ru sites for oxygen adsorption, and in addition adsorbed water can transfer its H atom to Cl<sub>ot</sub> which then desorbs in the form of HCl.

Readsorption of  $\text{Cl}_2$  has an inhibiting effect on oxygen adsorption because dissociative  $\text{Cl}_2$  adsorption blocks two active 1f-cus Ru sites. These processes underline the character of the HCl oxidation as a reaction close to equilibrium.

Altogether, the one-dimensional type of catalyst, the strong chlorine adsorption, the strong interchange with the gas phase and ample experiments on the surface render the HCl oxidation reaction over  $\text{RuO}_2(110)$  an exciting playground for kMC simulations. In the following, we restrict ourselves to two specific aspects of the HCl oxidation for which ample experimental data are available. This is the process of formation of trapped oxygen on the  $\text{RuO}_2(110)$  surface during the HCl oxidation reaction<sup>73</sup> and the chlorination of stoichiometric  $\text{RuO}_2(110)$  by HCl exposure at higher temperatures.

### 3.3.2 One dimensionality in the HCl Oxidation over $\text{RuO}_2(110)$

The catalytically active 1f-cus Ru sites form one-dimensional rows at the  $\text{RuO}_2(110)$  surface. If reaction intermediates adsorbed on the 1f-cus sites cannot be exchanged across the bridging oxygen rows, then the 1f-cus Ru sites constitute a catalyst with one-dimensional confinement. In a dedicated coadsorption experiment of oxygen and HCl, it has been shown that this one-dimensionality causes single surface  $\text{O}_{\text{ot}}$  atoms to be trapped by  $\text{Cl}_{\text{ot}}$  atoms, so that surface oxygen is not able to desorb from the  $\text{RuO}_2(110)$  surface at the expected temperature of 420 K.<sup>30</sup> Trapped oxygen needs desorption temperatures as high as 700 K to form  $\text{O}_2$ . Due to the one-dimensional character of this surface reaction, a simple mean field approach cannot be applied for modeling this coadsorption experiment, but rather kinetic Monte Carlo (kMC) simulations are required.<sup>73</sup> The steric hindrance of oxygen desorption may have profound implication on the reaction kinetics, allowing for configurational control in catalysis.<sup>74</sup>

On a stoichiometric  $\text{RuO}_2(110)$  surface, trapped oxygen on the 1f-cus Ru rows was experimentally prepared by co-exposure of HCl and  $\text{O}_2$ . The surface was exposed to 1.5 L of HCl at a temperature of  $T = 420$  K. During sample cooling from  $T = 350$  K to room temperature, 5 L of  $\text{O}_2$  (1 L corresponds to a dose of 1.33 mbar's) were co-dosed, thereby saturating the HCl-pre-exposed surface with  $\text{O}_{\text{ot}}$ . Fig. 7b shows the subsequent temperature programmed desorption (TPD) signals of  $\text{O}_2$  ( $m/e = 32$ ) and  $\text{Cl}_2$  ( $m/e = 70$ ).

The energy parameters for the experiment-based kMC simulations of adsorption, desorption and reaction can be found in **Table 1** of Ref. 73. First the exposure process of 1.5 L of HCl at 420 K to the  $\text{RuO}_2(110)$  surface was simulated by kMC. HCl adsorbs dissociatively, forming on-top Cl ( $\text{Cl}_{\text{ot}}$ ) and bridging hydroxyl groups ( $\text{O}_{\text{br}}\text{H}$ ). The kMC

derived distribution of  $\text{Cl}_{\text{ot}}$  and  $\text{O}_{\text{br}}\text{H}$  is shown in Fig. 7a. Onto this surface, the exposure of 5 L of  $\text{O}_2$  at room temperature is simulated with the result that most of the vacant 1f-cus Ru sites are occupied by on-top O (cf. Fig. 7a). If  $\text{O}_{\text{ot}}$  directly faces a bridging  $\text{O}_{\text{br}}\text{H}$  species, then hydrogen transfer takes place to form  $\text{O}_{\text{ot}}\text{H}$  and finally on-top water  $\text{O}_{\text{ot}}\text{H}_2$  (consistent with experiments<sup>75</sup>). As can be seen in Fig. 7a the number of on-top O and water species between two neighboring  $\text{Cl}_{\text{ot}}$  species is always even.

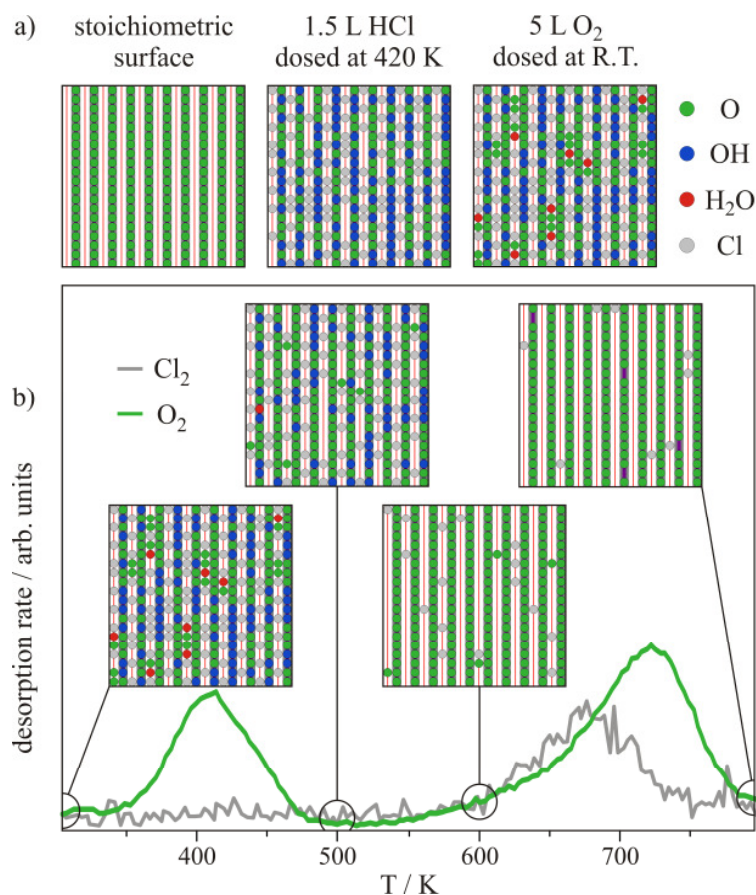


**Fig. 7:** KMC simulations of temperature programmed (TPR) reaction experiments starting from a  $\text{RuO}_2(110)$  surface which was exposed to 1.5 L of HCl at 420 K, followed by 5 L of  $\text{O}_2$  at 298 K. The change in the surface configuration is simulated as the temperature is increased from 298 K to 750 K with a linear temperature ramp (5 K/s)<sup>73</sup>. The grey/purple rows indicate the bridging position where for the case of stoichiometric  $\text{RuO}_2(110)$  bridging O sits. The red lines are the rows of 1f-cus Ru sites. Color code: green = O, grey = Cl, red =  $\text{OH}_2$ , blue = OH. Copyright © 2012 Elsevier.

With this “prepared” surface, a TPR experiment (temperature ramp 5 K/s) was simulated, and snapshots of the configurations at certain temperatures were extracted (cf. Fig. 7b). First, annealing to 500 K leads to desorption of on-top O by recombination of neighboring  $\text{O}_{\text{ot}}$  and desorption of most of the water molecules. Most of the  $\text{O}_{\text{ot}}$  species are

already trapped in between two adjacent  $\text{Cl}_{\text{ot}}$ . Part of the bridging hydroxyl groups have been transformed to  $\text{O}_{\text{br}}$  by hydrogen transfer to on-top Cl and instantaneous desorption of HCl.

On heating the sample to 600 K,  $\text{Cl}_{\text{ot}}$  atoms diffuse along the 1f-cus Ru rows, picking up the residual hydrogen from  $\text{O}_{\text{br}}\text{H}$  and desorbing as HCl. This process leads to a hydrogen-free surface with trapped  $\text{O}_{\text{ot}}$  atoms, which are locked in by two adjacent  $\text{Cl}_{\text{ot}}$  species. Increasing the sample temperature to 800 K leads to the desorption of the trapped oxygen and the formation of bridging O vacancies. Concomitantly, most of the  $\text{Cl}_{\text{ot}}$  atoms desorb recombinatively. A few of the  $\text{Cl}_{\text{ot}}$  atoms, which cannot desorb, remain on the surface, but can be incorporated into the bridging vacancies.<sup>64-66</sup> With an HCl exposure of 1.5 L, the total ratio of on-top O desorbing at 420 K and those at 700 K is 1:1, roughly reconciling the experimentally found ratio in TPR. The number of produced  $\text{Cl}_2$  molecules equals the number of oxygen molecules produced from trapped O.

### 3.3.3 The process of surface chlorination of $\text{RuO}_2(110)$ : Towards DFT-based kMC

The previous example in chapter 3.3.2 showed the successful application of experiment-based kMC to one aspect of the HCl oxidation over  $\text{RuO}_2(110)$ . To gain new insight into the reaction under steady-state conditions, a DFT-based parameter set was introduced which included lateral interactions using the method of Cluster Expansion.<sup>13, 76</sup> Our final parameter set is based on over 200 different configurations and contains about 100 parameters. It includes pairwise lateral interactions up to third-nearest neighbor, three-body interactions and hydrogen bonds for OH and  $\text{OH}_2$  species.

As an example for practical application of such a DFT-based parameter set, we will simulate the process of surface chlorination of  $\text{RuO}_2(110)$  in pure HCl at various degrees of initial surface hydrogenation. For the chlorination of  $\text{RuO}_2(110)$  starting from a stoichiometric surface, the following mechanism has been proposed on the basis of dedicated coadsorption experiments:<sup>65,66</sup> HCl molecules adsorb dissociatively on-top of 1f-cus-Ru, transferring hydrogen to  $\text{O}_{\text{br}}$ , thereby forming bridging water. When  $\text{O}_{\text{br}}\text{H}_2$  desorbs, the vacancy is filled by Cl, thereby forming  $\text{Cl}_{\text{br}}$ .<sup>64,65</sup> It was found experimentally that the chlorination is promoted by dosing  $\text{H}_2$  at room temperature prior to HCl exposure, yielding a higher degree of chlorination in a TPR experiment than without pre-dosing  $\text{H}_2$ .<sup>65</sup>

We investigated the effect of  $\text{H}_2$  pre-exposure on the chlorination kinetics under steady-state conditions at  $T = 473$  K and  $p(\text{HCl}) = 10^{-5}$  mbar using our DFT-based parameter set.<sup>76</sup> Fig. 8a shows the chlorination curves for various pre-coverages ( $\theta_{\text{O}}(\text{O}_{\text{br}}\text{H}) = 0, 0.2, 0.4, 0.6, 0.8, 1.0$  and  $\theta_{\text{O}}(\text{O}_{\text{br}}) = 1 - \theta_{\text{O}}(\text{O}_{\text{br}}\text{H})$ ). The different slopes of each curve close to  $t = 0$  indicate

that the initial chlorination rate depends strongly on  $\theta_0(\text{O}_{\text{br}}\text{H})$ , with the highest  $\theta_0(\text{O}_{\text{br}}\text{H})$  yielding the highest initial chlorination rate. As HCl exposure time advances and the chlorination degree increases, the chlorination rate drops until it reaches a plateau.

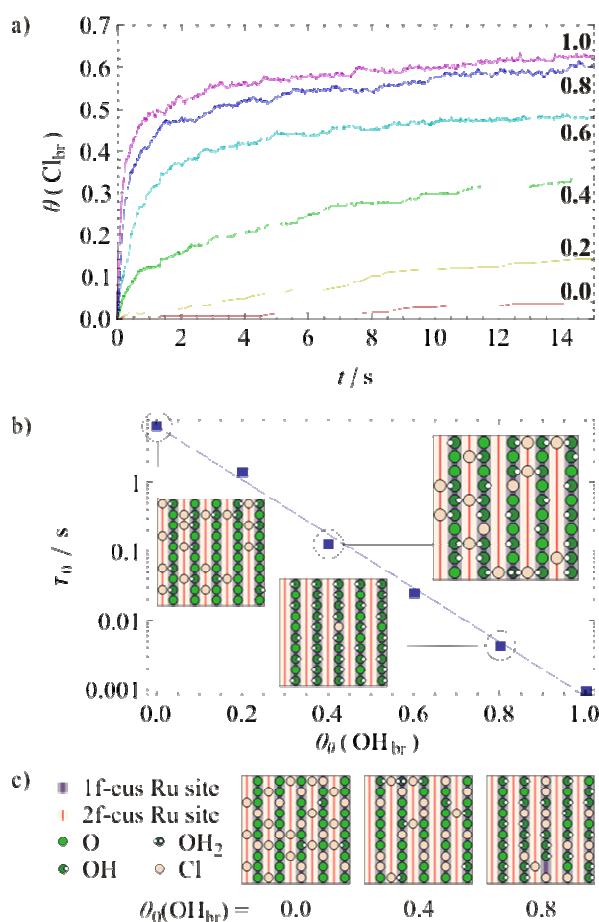


**Fig. 8:** KMC simulations of the surface chlorination of  $\text{RuO}_2(110)$  at 473 K and  $p(\text{HCl}) = 10^{-5}$  mbar on a  $24 \times 24$  lattice; **a)** Time evolution of surface chlorination for various pre-coverages of H. The starting coverage  $\theta_0(\text{O}_{\text{br}}\text{H})$  is indicated in bold numbers close to the curve; **b)** The logarithm of the induction time  $\tau_0$  for the chlorination follows a roughly linear relationship with  $\theta_0(\text{O}_{\text{br}}\text{H})$ . The trend can be approximated by  $\ln(\tau_0/s) = 1.9 - 9.0 \theta_0(\text{O}_{\text{br}}\text{H})$ . Configurations after induction are shown for  $\theta_0(\text{O}_{\text{br}}\text{H}) = 0.0, 0.2, 0.4$ ; **c)** shows configurations for  $\theta_0(\text{O}_{\text{br}}\text{H}) = 0.0, 0.4, 0.8$  for a fixed chlorination degree of the bridge positions of 0.25.

Plotting the degree of chlorination versus  $\log(\text{time})$  reveals an induction time  $\tau_0$ ; for details see supporting information (cf. Fig. S1). As shown in Fig. 8b the logarithm of  $\tau_0$  declines linearly with  $\theta_0(\text{O}_{\text{br}}\text{H})$ . The higher  $\theta_0(\text{O}_{\text{br}}\text{H})$ , the more likely it is for an HCl molecule to adsorb next to an existing  $\text{O}_{\text{br}}\text{H}$  group and the more likely it is for two neighboring  $\text{O}_{\text{br}}\text{H}$  groups to recombine and form water. Therefore, a higher  $\theta_0(\text{O}_{\text{br}}\text{H})$  results in faster chlorination.

To a first approximation, the maximum degree of chlorination is 1. Because the formation of water in bridge position requires two HCl to adsorb; two  $\text{Cl}_{\text{ot}}$  are also formed.

One of them becomes  $\text{Cl}_{\text{br}}$  by hopping into the vacancy after desorption of  $\text{H}_2\text{O}_{\text{br}}$ . The other chlorine atom is left on the 1f-cus row as  $\text{Cl}_{\text{ot}}$ . When  $\text{Cl}_{\text{ot}}$  accumulates at the surface during chlorination, further adsorption of HCl is inhibited. This means that the recombination of  $\text{Cl}_{\text{ot}}$  to form  $\text{Cl}_2$  becomes rate-limiting for the chlorination process of  $\text{RuO}_2(110)$  when  $\text{O}_{\text{br}}\text{H}$  groups have been diminished and  $\text{Cl}_{\text{ot}}$  has accumulated. At 473 K and  $p(\text{HCl}) = 10^{-5}$  mbar, the coverage of  $\text{Cl}_{\text{ot}}$  cannot exceed 1/3 due to repulsive lateral interactions.

Fig. 8c shows configurations for  $\theta_0(\text{O}_{\text{br}}\text{H}) = 0.0, 0.4, 0.8$  at a chlorination degree of 0.25. For  $\theta_0(\text{O}_{\text{br}}\text{H}) = 0.0$ , the coverage of  $\text{Cl}_{\text{ot}}$  is approximately 1/3, suggesting that the chlorination rate is kinetically controlled by the recombination of  $\text{Cl}_{\text{ot}}$ . In the case of  $\theta_0(\text{O}_{\text{br}}\text{H}) = 0.4$ , a low  $\text{Cl}_{\text{ot}}$  coverage indicates that desorption of  $\text{Cl}_2$  is not rate-controlling. A low hydrogenation degree of the  $\text{O}_{\text{br}}$  suggests rather that the adsorption of HCl, which transforms  $\text{O}_{\text{br}}$  to  $\text{O}_{\text{br}}\text{H}$ , is rate-limiting. A different picture emerges for  $\theta_0(\text{O}_{\text{br}}\text{H}) = 0.8$ , where  $\theta(\text{Cl}_{\text{ot}})$  is quite low, while  $\theta(\text{O}_{\text{br}}\text{H})$  is high. This configuration suggests that the formation of  $\text{O}_{\text{br}}\text{H}_2$  by recombination of neighboring  $\text{O}_{\text{br}}\text{H}$  is the rate-limiting step.

#### 4. Concluding remarks

Major objectives in molecular catalysis research concern the establishment of the reaction mechanism of a catalyzed chemical reaction as well as the identification of the active sites/phases on the catalyst and potential bottlenecks in the catalyzed reaction. Kinetic data in the form of activity data such as turnover frequencies (TOF) as a function of temperature and/or partial pressures lay down the basis for a subsequent kinetic analysis by first suggesting a reasonable reaction mechanism, i.e., a complete sequence of elementary reaction steps by which the desired product is formed. TOF values derived from kinetic models that account for the intricate interplay of the elementary reaction steps can be compared to the experimental data in order to support or rule out the proposed mechanism.

Within the transition state theory, the kinetics of each of the proposed elementary steps is determined by the activation energy and the frequency factor. Phenomenological microkinetic modeling relies on the tacit assumption that only the averaged surface coverages of reaction intermediates enter the differential rate equations.<sup>1</sup> This so-called mean field approximation is appropriate only if the reactants form an ideal mixture on the surface<sup>4</sup> which, however, is often not met in real systems where strong lateral interactions and statistical correlations are operative between the adsorbed reactants. In phenomenological kinetic modeling, the activation energies and frequency factors are mostly retrieved by varying these parameters systematically (or with an optimization routine) within the proposed reaction

mechanism to obtain the best fit to the experimental kinetic data. However, without extensive prior knowledge, this inverse problem is ill-defined and easily leads to erroneous conclusions. Therefore, molecular modeling best resorts to model catalysts, for which the complexity of the real catalytic system is substantially reduced and adopted to the scientific question in mind. Elementary reaction steps can be identified with modern surface science techniques including scanning tunneling microscopy (STM), atomic force microscopy (AFM), and in-situ spectroscopic methods. The activation barriers can be determined by analyzing temperature programmed reaction experiments of dedicated coadsorption experiments in which only few elementary processes are active at a time.<sup>21</sup>

An elaborate way to follow the progress of a catalytic reaction system - without relying on tacit assumptions such as the mean field approximation - is to carry out kinetic Monte Carlo simulations (kMC).<sup>4,11,12,77,78</sup> The most important ingredients are a complete list of elementary reaction steps together with corresponding activation barriers in various configurations. Of particular interest are the interaction energies between the reactants on the surface.<sup>79-81</sup> Without inclusion of such interaction energies, the temperature dependence of the catalyzed reaction cannot be properly accounted for.<sup>21, 62</sup> Lateral interaction energies are in general more difficult to derive, but the simulation of thermal desorption spectra is one approach to this problem. In-situ methods, such as RAIRS<sup>21</sup>, STM<sup>82</sup> HP-XPS<sup>83, 84</sup> can provide detailed information about the steady state surface configuration under reaction conditions which in turn can serve as a benchmark for kMC simulated snapshots of the surface configuration. This comparison can even be quantified by calculating the spectrum of such a surface configuration as exemplified with in-situ RAIRS experiments for the CO oxidation on RuO<sub>2</sub>(110).<sup>21</sup> RAIRS experiments indicate that the stretching frequency of adsorbed CO depends not only on the adsorption site but also sensitively on the local adsorption environment of the vibrating CO molecule. After systematic RAIRS experiments of the CO adsorption in a variety of well defined local environments have been performed, such as is the case with the CO oxidation over RuO<sub>2</sub>(110),<sup>45</sup> then the kMC simulated snapshots of the spatial distribution of reactants can directly be converted to a simulated RAIR spectrum which, upon comparison with the experimental RAIR spectra, would give an important feedback on the accuracy of the simulated configurations and, indirectly, on the reliability of the parameter set used.<sup>21</sup>

The experiment-based kMC<sup>21</sup> preferably requires a full set of experiments dedicated to the elementary reaction steps. These requirements can be met for relatively simple reaction systems such as the CO oxidation on RuO<sub>2</sub>(110), but this approach becomes prohibitively

time-consuming when focusing on more complex reactions. Therefore, kMC methods can be combined with electronic structure calculations of the activation energies and entropies involved in the elementary processes.<sup>41, 48, 85</sup> Of course, also the 'ab-initio' approach needs the prior knowledge of the nature of the active sites and a complete set of elementary steps.

If results from kMC simulations are only compared with kinetic reaction data, the conclusions are not clear-cut, since several parameter sets can fit the experimental data equally well. As demonstrated with the CO oxidation on RuO<sub>2</sub>(110),<sup>49</sup> three different parameter sets are equally able (or unable) to describe the kinetic data. Instead of the simple kinetic reaction data, the configuration of reactants on the catalyst's surface may serve as a benchmark when comparing kMC results to experiment. For the case of CO oxidation, at least one parameter set for DFT-based kMC could clearly be ruled out on the basis of the simulated surface configurations.<sup>49</sup> However, the other two parameter sets discussed in this perspective (Kiejna and Seitsonen) can not be discriminated on the basis of surface configurations at a specific reaction condition. Here, a promising way to differentiate between these data sets of Kiejna and Seitsonen would be to identify with kMC simulations reaction parameters, where the differences in configurations will lead to significantly different RAIR spectra and then measure RAIRS spectra for such conditions. Actually, simple experiments under steady state conditions are not sufficient but rather transient experiments are called for to discriminate different input parameter sets in kMC simulations. The surface configurations in the transient regime of the reaction until steady state is reached are much more sensitive to the actual kinetics of the elementary reaction steps than steady state configurations. From an experimental point of view important is the fact that at 325 K the kinetics of the CO oxidation over RuO<sub>2</sub>(110) is so slow that the transient region of the reaction can readily be time resolved by in-situ RAIRS experiments.

An efficient means of microkinetic modelling of a surface reaction is based on a mean field approach, where the reaction rate for the surface recombination process is proportional to the product of surface coverages of the reactants. However, this assumption is frequently not met on the catalyst surface, as pointed out by Ertl and Engel.<sup>8, 9</sup> Kinetic MC is superior over MF when heterogeneities are present on the surface, such as phase separation, ordering of the reaction intermediates, dimensional confinement and also high diffusion barriers. Therefore, the mean field approach may break down when pronounced anisotropy is encountered in a system in the form of one-dimensional confinement, such as observed with the HCl oxidation over RuO<sub>2</sub>(110).<sup>73</sup>

Recently, the differences of results obtained from MF and kMC based microkinetic methods have been critically compared.<sup>60,61</sup> It turned out that TOF values determined by these methods can easily deviate by several orders of magnitude for a wider range of significant CO oxidation reaction conditions on RuO<sub>2</sub>(110) due to strong site correlations. However, these studies ignored the interaction among the reactant intermediates on the surface which is a weak point of this study as strong site correlations are sensitively affected by lateral interactions. Indeed, a direct comparison of MF and kMC methods including lateral interactions clearly demonstrates that the TOF values derived by MF and kMC are quite similar over a wide range of reaction conditions.

What are the current shortcomings of kMC simulations? First of all, there is the completeness of the proposed reaction mechanism. Are all elementary reaction steps included in the reaction mechanism? A second point concerns the accuracy of the input parameters, in particular the activation energies of the elementary steps. With DFT-based kMC, the obtained accuracy is no better than 20-30 kJ/mol.<sup>43,55</sup> These uncertainties make a quantitative comparison with experimental TOF values difficult if not even impossible. Limited accuracy is, however, not just a quantitative matter but is mandatory for a qualitative discussion as accuracy of DFT calculations must be high enough to discriminate various reaction mechanisms and to recognize whether an elementary step in the mechanism is missing when compared with appropriate experiments. Even worse, as shown by the kMC simulations using Kiejna and Reuter parameter sets,<sup>49</sup> the surface configurations under CO oxidation reaction conditions are completely different, although the energy differences do not exceed 20-30 kJ/mol. In this example, the overall reaction mechanism (if defined as the selectivity between possible parallel elementary steps) changes if the parameter in question is slightly modified, drastically altering the distribution of intermediates on the surface.

Although the interaction energies between the reaction intermediates are of the same order as the uncertainties in the energy barriers, a complete neglect of lateral interaction in kMC should be a “no go” in present kMC simulations since even such basic properties like the apparent activation energy cannot be reconciled, as demonstrated with the CO oxidation on RuO<sub>2</sub>(110)<sup>49</sup> and on Pt(111).<sup>86</sup> In order to assess the quality of a kMC simulation, i.e., the appropriateness of the proposed reaction mechanism and the reliability of the input parameter set, one needs to compare the simulated results with as many experiments as possible, including kinetic data and most notably in-situ spectroscopic data.

However, we should note that experimental TOF values are also subject to large errors. The reasons for the large uncertainties of experimental TOF values is traced back to

uncertainties in the number of active sites and the unknown sensitivity variation of the mass spectrometer, for instance to the product CO<sub>2</sub> when pure CO<sub>2</sub> is replaced by a gas mixture of CO<sub>2</sub>, O<sub>2</sub> and CO. In general, the batch reactors<sup>87</sup> and flow reactors<sup>88</sup> in surface chemistry do not run isothermally as assumed in kMC. This may lead to systematic deviations of kMC simulations and kinetic experiments. Therefore, the experimental TOF values are not very precisely known, although variations of TOF as a function of reaction conditions are considered to be significantly more reliable. High pressure in-situ experiments may face limitations due to mass and heat transfer. These limitations are not incorporated in kMC simulations and may therefore lead to wrong conclusions. One possible way to overcome this problem could be the combination of kMC simulations with fluid-dynamical equations as proposed by Reuter et al.<sup>16</sup>. In this way, one can try to retrieve the true underlying reaction kinetics from mass and/or heat limited kinetic data. In general, this inverse problem is again mathematically ill-defined when the catalytic reaction is mass and heat transfer limited. However, if in addition to kinetic data the gas phase composition above the model catalyst can be monitored in-situ with a spatial resolution of sub mm, then true kinetic data can be retrieved from this combined approach even if the reaction is mass flow controlled.<sup>89</sup>

What are the obvious benefits of kMC simulation for catalysis research? There is a clear educational impact of kMC on catalysis research in that the complex interplay of elementary steps visualized by kMC can deepen our understanding of the underlying processes and their correlation. This depth of understanding can only be achieved on model catalysts with limited structural complexity and for which DFT calculations are tractable. KMC simulations are able to assess a proposed reaction mechanism by comparing the simulated data with an extended set of experimental data, either kinetic or spectroscopic. In a next step, one may be interested in the extrapolation of these findings to practical catalysts materials under practical reaction conditions. Model catalysis faces two essential problems here, which are coined as pressure and materials gaps. In general, model catalysis is performed under relatively low pressure conditions (10<sup>-10</sup> mbar – 10 mbar), while practical reactions run at 1...100 bar. The materials gap comes into play when the catalytic reaction is highly structure sensitive, i.e., when the reaction mechanism critically depends on the particular facets of the nanoparticle or on step and kinks. This means that the nanoparticles of the active catalyst component behave differently to the single crystalline surface considered in model catalysis. If there is a materials gap, then the model system has to be properly adopted to capture the essentials of the catalytically active sites of the supported nanoparticles of the active component. This may be, for instance, the interaction of the particle with the support. Consequently, one should

consider nanoparticles on structurally well-defined oxide films as proper model catalysts.<sup>90</sup> Or in the case that steps and kinks are the most important catalytic sites of the catalysts, one should resort to vicinal surfaces with ordered arrays of steps and kinks.<sup>91</sup> If various facets of the nano particles contribute differently to the overall reaction, then one needs to study the reaction on different well-defined orientations of the catalytic material and combining then the results in terms of the Wulff construction to get the full picture of the reaction. Therefore in principle, the materials gap can be bridged. However, this kind of kMC simulation is much more involved.<sup>92</sup>

However, assuming that no materials gap is faced, the pressure gap can be bridged by kMC simulations as demonstrated with the CO oxidation on RuO<sub>2</sub>(110).<sup>21, 49</sup> For the case of ammonia synthesis over Fe-based catalysts, this pressure gap has been successfully bridged by MK. Most of the elementary reaction steps have been determined by Ertl and coworkers under ultrahigh vacuum (UHV) conditions,<sup>93</sup> while the extrapolation of the reaction kinetics to practical conditions (200-300 bar,  $T = 600-800$  K) was successfully carried out by Stoltze and Norskov<sup>7</sup> and by Bowker et al..<sup>94</sup>

#### Acknowledgement:

We thank Attila Farkas for fruitful discussions in particular at the beginning of this kMC project. JLU is acknowledged for a graduate stipend for Franziska Hess. This project was partly supported by the German Science council (DFG) and the federal ministry of science and education (BMBF\_Deacon: 033R018C).

#### References:

1. K.J. Laidler, *Chemical Kinetics*, Harper & Row, New York, (1987).
2. G. Ertl, H. Knözinger, F. Schüth, and J. Weitkamp (Eds.) *Handbook of Heterogeneous Catalysis*; Wiley New York, 2008.
3. M. Boudart, *Kinetics of Chemical Processes*, Prentice Hall, Englewood Cliffs, NJ, 1968.
4. Stoltze, P., *Prog. Surf. Sci.* 2000, **65**, 65.
5. G. Ertl. *Angew. Chem. Int. Ed.* 2008, **47**, 3524.
6. C.B. Duke, E.W. Plummer (eds.) *Surf. Sci.*, 2002, **500** Special Issue: Frontiers in Surface and Interface Science.
7. P. Stoltze, J.K. Norskov, *Phys. Rev. Lett.* 1985, **25**, 2502.
8. T. Engel and G. Ertl *Adv. Catal.*, 1979, **28**, 1.
9. G. Ertl, *Adv. Catal.*, 1991, **37**, 213.

10. G. Ertl, Reactions at Solid Surfaces, John Wiley & Sons Inc., Hoboken, New Jersey, 2009.
11. D. T. Gillespie, *J. Comput. Physics*, 1976, **22**, 403.
12. A. B. Bortz, M. H. Kalos, and J. L. Lebowitz, *J. Comput. Phys.*, 1975, **17**, 10.
13. A.P.J. Jansen, Lecture Notes in Physics, Springer, Berlin, 2012.
14. M. Stamatakis and D.G. Vlachos, *ACS Catal.*, 2012, **2**, 2648.
15. J.A. Keith, J. Anton, P. Kaghazchi, T. Jacob in *Modeling and Simulation of Heterogeneous Reactions*, Ed. O. Deutschmann, Wiley, VCH 2012, 1.
16. M.K. Sabbe, M.-F. Reyniers, and K. Reuter, *Catal. Sci. Technol.*, 2012, **2**, 2010-2024.
17. I. Chorkendorff, and J. W. Niemantsverdriet, Concepts of Modern Catalysis and Kinetics, Wiley-VCH, Weinheim (2003).
18. R.M. Krupka et al, *Trans. Faraday Soc.*, 1966, **62**, 2754.
19. Gillespie, D. T. (1992). "Markov processes: an introduction for physical scientists". Boston, Academic Press, chapter 5.
20. A.P.J. Jansen, *Computer Phys. Commun.*, 1995, **86**, 1.
21. A. Farkas, F. Hess, and H. Over, *J. Phys. Chem, C*, 2012, **116**, 581.
22. H. Over, *Chem. Rev.*, 2012, **112**, 3356.
23. D. Teschner, R. Farra, L.D. Yao, R. Schlogl, H. Soerijanto, R. Schomaecker, T. Schmidt, L. Szentmiklosi, A.P. Amrute, C. Mondelli, J. Perez-Ramirez, G. Movell-Leruth, N. Lopez, *J. Catal.* 2012, **285**, 273.
24. H. Over, *J. Phys. Chem. C*, 2012, **116**, 6779.
25. H. Over, *Appl. Phys. A*, 2002, **75**, 37.
26. C.Y. Fan, J. Wang, K. Jacobi, G. Ertl, *J. Chem. Phys.* 2001, **114**, 10058.
27. H. Over, A.P. Seitsonen, E. Lundgren, M. Schmid, P. Varga, *J. Am. Chem. Soc.* 2001, **123** 11807.
28. J. Wang, C.Y. Fan, K. Jacobi, and G. Ertl, *J. Phys. Chem. B*, 2002, **106**, 3427.
29. Y.D. Kim, A.P. Seitsonen, and H. Over, *H. Phys. Rev. B*. 2001, **63**, 5419.
30. Y.D. Kim, A.P. Seitsonen, S. Wendt, J. Wang, C. Fan, K. Jacobi, H. Over, and G. Ertl, *G. J. Phys. Chem. B*, 2001, **105**, 3752.
31. S. Wendt, A.P. Seitsonen, Y.D. Kim, M. Knapp, H. Idriss, and H. Over, *Surf. Sci.*, 2002, **505**, 137.
32. K. Reuter and M. Scheffler, *Phys. Rev. B*, 2003, **68**, 045407.
33. H. Wang and W.F. Schneider, *J. Chem. Phys.*, 2007, **127**, 064706.
34. S. Wendt, M. Knapp, and H. Over, *J. Am. Chem. Soc.*, 2004, **126**, 1537.
35. A. Kiejna, G. Kresse, J. Rogal, A. De Sarkar, K. Reuter, and M. Scheffler, *M. Phys. Rev. B.*, 2006, **73**, 035404.
36. A.P. Seitsonen and H. Over, *Surf. Sci.*, 2009, **603**, 1717.
37. H. Over, and M. Muhler, *Prog. Surf. Sci.*, 2003, **72**, 3.

38. A. Böttcher and H. Niehus, *Phys. Rev. B*, 1999, **60**, 14396.
39. A.P. Seitsonen, Y.D. Kim, M. Knapp, S. Wendt, and H. Over, *Phys. Rev. B*, 2002, **65**, 035413.
40. S.H. Kim and J. Wintterlin *J. Phys. Chem B*, 2004, **108**, 14565.
41. K. Reuter and M. Scheffler, *Phys. Rev. B*, 2006, **73**, 045433.
42. S. Wendt, A.P. Seitsonen, and H. Over, *Catal. Tod.*, 2003, **85**, 167.
43. J.K. Norskov, T. Bligaard, J. Rossmeisl, and C.H. Christensen, *Nat. Chem.*, 2009, **1**, 37.
44. M. Neurock, *Ind. Eng. Chem. Res.* 2010, **49**, 10183.
45. A. Farkas, G. Mellau, and H. Over, *J. Phys. Chem., C* 2009, **113**, 14341.
46. J. Assmann, V. Narkhede, N. A. Breuer, M. Muhler, A. P. Seitsonen, M. Knapp, D. Crihan, A. Farkas, G. Mellau, and H. Over, *J. Phys. Condens. Matter* 2008, **20**, 184017.
47. K.A. Fichthorn and W.H. Weinberg, *J. Chem. Phys.*, 1991, **95**, 1090.
48. E.W. Hansen and M. Neurock, *J. Catal.*, 2000, **196**, 241.
49. F. Hess, A. Farkas, A.P. Seitsonen, and H. Over, *J. Comp. Chem.*, 2012, **33**, 757.
50. P. Blaha, K. Schwarz, P. Soratin, S.B. Trickey, *Comput. Phys. Commun.* 1990, **59**, 399.
51. K. Schwarz, P. Blaha, *Comput. Mater. Sci.* 2003, **28**, 259.
52. G. Kresse and J. Furthmüller, *Comput. Mater. Sci.*, 1995, **6**, 15.
53. P. Blöchl, *Phys. Rev. B* 1994, **50**, 17953.
54. J. P. Perdew, K. Burke, and M. Ernzerhof, *Phys. Rev. Lett.*, 1996, **77**, 3365.
55. P. J. Feibelman, *Top. Catal.*, 2010, **53**, 417
56. R. M. Ziff, E. Gulari, and Y. Barshad, *Phys. Rev. Lett.*, 1986, **56**, 2553.
57. H. Over, O. Balmes, and E. Lundgren, *Catal. Tod.*, 2009, **145**, 236.
58. H. Over, O. Balmes, and E. Lundgren, *Surf. Sci.*, 2009, **603**, 298.
59. <http://www.uni-giessen.de/cms/fbz/zentraledateien/kMCMovies>
60. B. Temel, H. Meskine, K. Reuter, M. Scheffler, and H. Metiu, *J. Chem. Phys.*, 2007, **126**, 204711.
61. S. Matera, H. Meskine, and K. Reuter, *J. Chem. Phys.*, 2011, **134**, 064713.
62. F. Hess and H. Over, *to be submitted*.
63. A. Hellman and K. Honkala, *J. Chem. Phys.*, 2007, **127**, 194704.
64. D. Crihan, M. Knapp, S. Zweidinger, E. Lundgren, C.J. Weststrate, J.N. Andersen, A.P. Seitsonen, H. Over, *H. Angew. Chem. Int. Ed.*, 2008, **47**, 2131.
65. J.P. Hofmann, S. Zweidinger, M. Knapp, A.P. Seitsonen, K. Schulte, J.N. Andersen, E. Lundgren, H. Over, *J. Phys. Chem. C*, 2010, **114**, 10901.
66. J.P. Hofmann, S. Zweidinger, A.P. Seitsonen, A. Farkas, M. Knapp, O. Balmes, E. Lundgren, J.N. Andersen, H. Over, *Phys. Chem. Chem. Phys.*, 2010, **12**, 15358.

67. S. Zweidinger, D. Crihan, M. Knapp, J.P. Hofmann, A.P. Seitsonen, E. Lundgren, C.J. Weststrate, J.N. Andersen, H. Over, *H. J. Phys. Chem. C*, 2008, **112**, 9966.
68. A. Lobo, H. Conrad, *Surf. Sci.*, 2003, **523**, 279.
69. M. Knapp, D. Crihan, A.P. Seitsonen, E. Lundgren, A. Resta, J.N. Andersen, H. Over, *J. Phys. Chem. C*, 2007, **111**, 5363.
70. N. Lopez, J. Gomez-Segura, R.P. Marin, J. Perez-Ramirez, *J. Catal.* 2008, **255**, 29.
71. S. Zweidinger, J.P. Hofmann, O. Balmes, E. Lundgren, H. Over. *J. Catal.* 2010, **272**, 169.
72. F. Studt, F. Abild-Pedersen, H.A. Hansen, I.C. Man, J. Rossmeisl, T. Bligaard, *Chem. Cat. Chem.*, 2010, **2**, 98.
73. F. Hess, P. P. T. Krause, S. F. Rohrlack, J. P. Hofmann, A. Farkas, H. Over, *Surf. Sci. Lett.*, 2012, **606**, L69.
74. W.F. Schneider, *Surf. Sci.*, 2012, **606**, 1351.
75. M. Knapp, D. Crihan, A.P. Seitsonen, H. Over, *J. Am. Chem. Soc.*, 2005, **127**, 3236.
76. F. Hess and H. Over, *to be submitted*.
77. J. J. Lukkien, J. P. L. Segers, P. A. J. Hilbers, R. J. Gelten, and A. P. J. Jansen, *Phys. Rev. E*, 1998, **58**, 2598.
78. D.-J.Liu, and J. W. Evans, *J. Chem. Phys.* 2006, **124**, 154705.
79. M. Silverberg, and A. Ben-Shaul, *J. Stat. Phys.* 1988, **52**, 1179.
80. E. Hansen and M. Neurock, *Surf. Sci.* 1999, **441**, 410.
81. D.J. Schmidt, W. Chen, C. Wolverton, W.F. Schneider, *J. Chem. Theory Comput.* 2012, **8**, 264.
82. J. Winterlin, S. Völkening, T. V. W. Janssens, T. Zambelli, and G. Ertl, *Science* 1997, **278**, 1931.
83. M. Salmeron, and R. Schlögl, *Surf. Sci. Rep.* 2008, **63**, 169.
84. R. Blume, M. Hävecker, S. Zafeirotos, D. Teschner, E. Kleimenov, A. Knop-Gericke, R. Schlögl, A. Barinov, P. Dudin, M. Kiskinova, *J. Catal.* 2006, **239**, 354.
85. P. Ruggerone, C. Ratsch, and M. Scheffler, „Density-functional theory of epitaxial growth of metals“ in *The Chemical Physics of Solid Surfaces Vol. 8: Growth and Properties of Ultrathin Epitaxial Layers*, ed. D.A. By King, and D. P. Woodruff, Elsevier Science, Amsterdam p. 490 (1997).
86. V.P. Zhdanov and B. Kasemo, *Appl. Surf. Sci.*, 1994, **74**, 147.
87. O. Balmes, R. van Rijn, D. Wermeille, A. Resta, L. Petit, H. Isern, T. Dufrane, R. Felici, *Cat. Tod.* 2009, **145**, 220.
88. R. van Rijn, M.D. Ackermann, O. Balmes, T. Dufrane, A. Geluk, H. Gonzalez, H. Isern, E. de Kuyper, L. Petit, V.A. Sole, D. Wermeille, R. Felici, J.W.M. Frenken, *Rev. Sci. Instrum.* 2010, **81**, 014101.
89. J. Zetterberg, S. Blomberg, J. Gustafson, Z.W. Sun, Z.S. Li, E. Lundgren, *Rev. Sci. Instrument.* 2012, **83**, 053104.
90. H. Kühlenbeck, S. Shaikhutdinov, H.-J. Freund, *Chem. Rev.* 2013, **113**, 3986.
91. H.C. Jeol, E.D. Williams, *Surf. Sci. Rep.* 1999, **34**, 171.

92. B.T. Loveless, C. Buda, M. Neurock, E. Iglesia, *J. Am. Chem. soc.* 2013, 135, 6107.
93. G. Ertl, *Critical Reviews in Solid State and Materials Science* 1982, **10**, 349.
94. M. Bowker, I. Parker, K.C. Waugh, *Surf. Sci.* 1988, **197**, L223.